ARTICLE Communicated by Eric Shea-Brown

Maximally Reliable Markov Chains Under Energy Constraints

Sean Escola
gse3@columbia.edu
Center for Theoretical Neuroscience and M.D./Ph.D. Program, Columbia University, New York, NY 10032, U.S.A.

Michael Eisele
mbjeisele@gmail.com
Kenneth Miller
ken@neurotheory.columbia.edu
Center for Theoretical Neuroscience, Columbia University, New York, NY 10032, U.S.A.

Liam Paninski
liam@stat.columbia.edu
Center for Theoretical Neuroscience and Department of Statistics, Columbia University, New York, NY 10032, U.S.A.

Signal-to-noise ratios in physical systems can be significantly degraded if the outputs of the systems are highly variable. Biological processes for which highly stereotyped signal generations are necessary features appear to have reduced their signal variabilities by employing multiple processing steps. To better understand why this multistep cascade structure might be desirable, we prove that the reliability of a signal generated by a multistate system with no memory (i.e., a Markov chain) is maximal if and only if the system topology is such that the process steps irreversibly through each state, with transition rates chosen such that an equal fraction of the total signal is generated in each state. Furthermore, our result indicates that by increasing the number of states, it is possible to arbitrarily increase the reliability of the system. In a physical system, however, an energy cost is associated with maintaining irreversible transitions, and this cost increases with the number of such transitions (i.e., the number of states). Thus, an infinite-length chain, which would be perfectly reliable, is infeasible. To model the effects of energy demands on the maximally reliable solution, we numerically optimize the topology under two distinct energy functions that penalize either irreversible transitions or incommunicability between states, respectively. In both cases, the solutions are essentially irreversible linear chains, but with upper bounds on the number of states set by the amount of available energy. We therefore conclude that a physical system for

which signal reliability is important should employ a linear architecture, with the number of states (and thus the reliability) determined by the intrinsic energy constraints of the system.

1 Introduction

In many physical systems, a high degree of signal stereotypy is desirable. In the retina, for example, the total number of G proteins turned on during the lifetime of activated rhodopsin following a photon absorption event needs to have a low variability to ensure that the resulting neural signal is more or less the same from trial to trial (Rieke & Baylor, 1998). If this were not the case, accurate vision in low-light conditions would not be possible. Biology offers a myriad of other examples where signal reproducibility or temporal reliability is necessary for proper function: muscle fiber contraction (Edmonds, Gibb, & Colquhoun, 1995b), action potential generation and propagation (Kandel, Schwartz, & Jessell, 2000), neural computations underlying motor control (Olivier, Davare, Andres, & Fadiga, 2007) or time estimation (Buhusi & Meck, 2005), ion channel and pump dynamics (Edmonds, Gibb, & Colquhoun, 1995a), circadian rhythm generation (Reppert & Weaver, 2002), cell-signaling cascades (Locasale & Chakraborty, 2008), and others. In some cases, it may be possible to reduce signal variability by making a system exceedingly fast, but in many cases, a nonzero mean processing time is necessary. The mechanism involved in the inactivation of rhodopsin, for example, needs to have some latency in order for enough G proteins to accumulate to effect the neural signal. In this article, we address the question of how to design a physical system that has a low signal variability while maintaining some desired nonzero mean total signal (and thus a nonzero mean processing time).

A previous numerical study of the variability of the signal generated during the lifetime of activated rhodopsin found that a multistep inactivation procedure (with the individual steps proposed to be sequential phosphorylations) was required to account for the low variability observed experimentally (Hamer, Nicholas, Tranchina, Liebman, & Lamb, 2003). This theoretical prediction was borne out when knockouts of phosphorylation sites in the rhodopsin gene were seen to result in increased variability (Doan, Mendez, Detwiler, Chen, & Rieke, 2006). These results led us to consider more generally whether a multistep system is optimal in terms of the reliability of an accumulated signal. Specifically, we limit ourselves to consider memoryless systems where the future evolution of the system dynamics depends on the current configuration of the system but not simultaneously on the history of past configurations. If such a memoryless system has a finite or countable number of distinct configurations (states) with near-instantaneous transition times between them, it can be modeled as a continuous-time Markov

chain. This class of models, though somewhat restricted, is sufficiently rich to adequately approximate a wide variety of physical systems, including the phosphorylation cascade employed in the inactivation of rhodopsin. By restricting ourselves to systems that can be modeled by Markov chains, our goal of identifying the system design that minimizes the variance of the total generated signal while maintaining some nonzero mean may be restated as the goal of determining the Markov chain network topology that meets these requirements given a set of state-specific signal accumulation rates.[1] This is the primary focus of the work presented here.

The article is organized as follows. In section 2, we review basic continuous-time Markov chain theory, introduce our notation, and review the necessary theory of the "hitting time," or first passage time, between two states in a Markov network. We then define a random variable to represent the total signal generated during the path between the first and last states in the network and show that this is a simple generalization of the hitting time itself. The squared coefficient of variation of this variable (the CV^2, or ratio of the variance to the square of the mean) will be our measure of the variability of the system modeled by the Markov chain. In section 3, we present our main theoretical result regarding the maximally reliable network topology. Simply stated, we prove that a linear Markov chain with transition rates between pairs of adjacent states that are proportional to the state-specific signal accumulation rates is optimal in that it minimizes the CV^2 of the total generated signal. In the special case that the state-specific signal accumulation rates are all equal to one, the total generated signal is the hitting time, and the optimally reliable solution is a linear chain with the same transition rate between all adjacent states (see Figure 1b). As an intermediate step, we also prove a general bound regarding the signal reliability of an arbitrary Markov chain (see equation 3.3), which we show to be saturated only for the optimal topology. In section 4, we numerically study the deviations from the optimal solution when additional constraints are applied to the network topology. Specifically, we develop cost functions that are meant to represent the energy demands that a physical system might be expected to meet. As the available "energy" is reduced, the maximally reliable structure deviates further and further from the optimal (i.e., infinite energy) solution. If the cost function penalizes a quantity analogous to the Gibbs free energy difference between states, then the resulting solution is composed of two regimes: a directed component, which is essentially an irreversible linear subchain, followed by a diffusive component, where the forward and backward transition rates between pairs of states along the chain become identical (see section 4.2). In the zero energy limit, the maximally reliable

[1] As we show, in the case that the state-specific signal accumulation rates are all unity, then the generated signal is the system processing time itself.

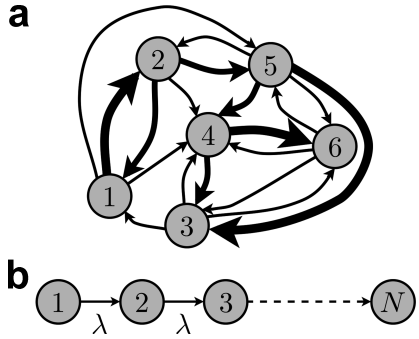

Figure 1: (a) Schematic of a six-state Markov chain. The circles and arrows represent the states and the transitions between states, respectively. The thicknesses of the arrows correspond to the values of the transition rates or, equivalently, the relative probabilities of transition. Nonexistent arrows (e.g., between states 2 and 3) reflect transition rates of zero. (b) A linear Markov chain with the same transition rate λ between all pairs of adjacent states in the chain (i.e., $\lambda_{i+1,i} = \lambda$). This topology uniquely saturates the bound on the CV^2 of the hitting time t_{1N} (see equation 3.1).

solution is purely diffusive, which is a topology amenable to analytic interpretation (see section 4.2.1). If instead the cost function penalizes all near-zero transition rates, then states are seen to merge until, at the minimum energy limit, the topology reduces to a simple two-state system (see section 4.3). In sections 4.4 and 4.5, we present a brief analytic comparison of the solutions given by the two energy functions to show that although they superficially seem quite different, they are in fact analogous. In both cases, the amount of available energy sets a maximum or effective maximum number of allowable states, and within this state space, the maximally reliable Markov chain architecture is a linear chain with transition rates between each pair of adjacent states that are proportional to the state-specific signal accumulation rates. Finally, in section 4.6, we argue that structure is necessary for reliability and that randomly connected Markov chains do not confer improved reliability with increased numbers of states. From this, we conclude that investing the energy resources needed to construct a linear Markov chain would be advantageous to a physical system.

2 Continuous Time Markov Chains

A Markov chain is a simple model of a stochastic dynamical system that is assumed to transition between a finite or countable number of states (see Figure 1a). Furthermore, it is memoryless—the future is independent of the past given the present. This feature of the model is called the Markov property.

In this article, we consider homogeneous continuous-time Markov chains. These are fully characterized by a static set of transition rates $\{\lambda_{ij} : \forall i, \forall j \neq i\}$ that describe the dynamics of the network, where λ_{ij} is the rate of transition from state j to state i. The dwell time in each state prior to a transition to a new state is given by an exponentially distributed random variable, which appropriately captures the Markovian nature of the system. Specifically, the dwell time in state j is given by an exponential distribution with time constant τ_j, where

$$\tau_j \equiv \frac{1}{\sum_{k \neq j} \lambda_{kj}}, \tag{2.1}$$

the inverse of the sum of all of the transition rates away from state j. Once a transition away from state j occurs, the probability $p_{j \to i}$ that the transition is to state i is given by the relative value of λ_{ij} compared to the other rates of transitions leaving state j. Specifically,

$$\begin{aligned} p_{j \to i} &= \frac{\lambda_{ij}}{\sum_{k \neq j} \lambda_{kj}} \\ &= \lambda_{ij} \tau_j. \end{aligned} \tag{2.2}$$

It is convenient to construct an $N \times N$ transition rate matrix to describe a homogeneous continuous-time Markov chain as follows:

$$\mathbf{A} \equiv \begin{pmatrix} q_1 & \lambda_{12} & \cdots & \lambda_{1N} \\ \lambda_{21} & q_2 & \cdots & \lambda_{2N} \\ \vdots & \vdots & \ddots & \vdots \\ \lambda_{N1} & \lambda_{N2} & \cdots & q_N \end{pmatrix}, \tag{2.3}$$

where $q_j = -1/\tau_j$. Note that each column of $\mathbf{A}$ sums to zero and that all off-diagonal elements (the transition rates) are nonnegative. The set of all $N \times N$ matrices of this form corresponds to the full set of N-state continuous-time Markov chains. For an introduction to the general theory of Markov chains, see, for example, Norris (2004).

2.1 Hitting Times and Total Generated Signals. In this article, we consider the reliability of the total signal generated during the time required for a Markovian system to arrive at state N given that it starts in state 1.[2] This time is often referred to as the hitting time, which can be represented by the random variable t_{1N}. The total generated signal, F_{1N}, can subsequently be defined in terms of the hitting time and the state-specific signal accumulation rates. If the rate of signal accumulation in state i is given by the

[2]States 1 and N are arbitrary, albeit convenient, choices. The labels of the states can always be permuted without changing the underlying network topology.

coefficient f_i, and the current state at time t is denoted $q(t)$, then we can define the total signal as

$$F_{1N} = \int_0^{t_{1N}} f_{q(t)}\, dt. \tag{2.4}$$

Note that in the case that $f_i = 1, \forall i$, the total generated signal equals the hitting time. The statistics of the random variables t_{1N} and F_{1N} are governed by the topology of the network, namely, the transition matrix $\mathbf{A}$. Our goal is to identify the network topology that minimizes the variance of the total signal and thus maximizes the reliability of the system, while holding the mean total signal constant.

Recall that the standard expression for the probability that a Markovian system that starts in state 1 is in state N at time t is given as

$$p(q(t) = N) = \mathbf{e}_N^T e^{\mathbf{A}t} \mathbf{e}_1, \tag{2.5}$$

where $\mathbf{e}_1 \equiv (1, 0, \ldots, 0)^T$ and $\mathbf{e}_N \equiv (0, \ldots, 0, 1)^T$ (i.e., the first and Nth standard basis vectors, respectively) (Norris, 2004). If the Nth column of $\mathbf{A}$ is a zero vector so that transitions away from state N are disallowed, making N a so-called collecting state of the system, then $p(q(t) = N)$ is equivalent to the probability that the hitting time t_{1N} is less than t. Assuming that this is true,[3] then the time derivative of equation 2.5 is the probability density of the hitting time itself:

$$p(t_{1N}) = \mathbf{e}_N^T \mathbf{A} e^{\mathbf{A}t_{1N}} \mathbf{e}_1. \tag{2.6}$$

Note that state N must be collecting in order for this distribution to integrate to 1. Additionally, $p(t_{1N})$ is well defined only if state N is both accessible from state 1 and is the only collecting state or collecting set of states accessible from state 1. We consider only topologies for which these three properties hold.

We can show that studying the statistics of the hitting time t_{1N} is equivalent to studying the statistics of the the total generated signal F_{1N} since the two random variables are simple transforms of each other. To determine the probability distribution of F_{1N}, we can consider the signal accumulation rates to simply rescale time. The transition rate λ_{ij} can be stated as the number of transitions to state i per unit of accumulated time when the system is in state j, and so the ratio λ_{ij}/f_j can similarly be stated as the number of transitions to state i per unit of accumulated signal when the system is

[3] Whether N truly is collecting or not does not affect the hitting time t_{1N} since this random variable is independent of the behavior of the system after arrival at state N. Thus setting the N^{th} column of $\mathbf{A}$ to zero does not result in a loss of generality.

in state j. Thus, by dividing each column of $\mathbf{A}$ by the corresponding signal accumulation rate, we can define the matrix $\tilde{\mathbf{A}}$ with elements $\phi_{ij} \equiv \lambda_{ij}/f_j$. Then the probability distribution of F_{1N} is given, by analogy with the hitting time distribution (see equation 2.6), as

$$p(F_{1N}) = \mathbf{e}_N^T \tilde{\mathbf{A}} e^{\tilde{\mathbf{A}} F_{1N}} \mathbf{e}_1. \tag{2.7}$$

Thus, for the remainder of the article, we focus solely on the reliability of a Markovian system as measured by the statistics of the hitting time rather than of the total generated signal (i.e., we consider $f_i = 1, \forall i$). This can be done without loss of generality since the results we present regarding the reliability of the hitting time can be translated to an equivalent set of results regarding the reliability of the total generated signal by a simple column-wise rescaling of the transition rate matrices.

2.2 The CV^2 as a Measure of Reliability. It is clear that given a Markov chain with a set of fixed relative transition rates, the reliability of the system should be independent of the absolute values of the rates (i.e., the scale) since a scaling of the rates would merely rescale time (e.g., change the units from seconds to minutes). Furthermore, the variance and the square of the mean of the hitting time t_{1N} would be expected to vary in proportion to each other given a scaling of the transition rates, since again this is just a rescaling of time. This can be demonstrated by noting, from equation 2.3, that scaling the rates of a Markov chain by the same factor is equivalent to scaling $\mathbf{A}$, since $\mathbf{A}$ is linear in the rates λ_{ij}, and, from equation 2.6, that scaling $\mathbf{A}$ is equivalent to rescaling t_{1N} and thus the statistics of t_{1N}. Therefore, we use the squared coefficient of variation (CV^2, or the dimensionless ratio of the variance to the square of the mean) to measure the reliability of a Markov chain and seek to determine the network topology (i.e., with fixed relative rates, but not fixed absolute rates), which minimizes the CV^2 and thus is maximally reliable.

3 Optimal Reliability

Intuitively, it seems reasonable that an irreversible linear chain with the same transition rate between all pairs of adjacent states (i.e., $\lambda_{i+1,i} = \lambda$ for all i and for some constant rate λ, and $\lambda_{ij} = 0$ for $j \neq i - 1$; see Figure 1b) may be optimal. For such a chain, the hitting time t_{1N} equals the sum from 1 to M (where we define $M \equiv N - 1$ for convenience) of the dwell times in each state of the chain $t_{i,i+1}$. This gives the CV^2 as

$$CV^2 \equiv \frac{\mathrm{var}(t_{1N})}{\langle t_{1N} \rangle^2}$$

$$= \frac{\mathrm{var}\left(\sum_{i=1}^{M} t_{i,i+1}\right)}{\left\langle \sum_{i=1}^{M} t_{i,i+1} \right\rangle^2}$$
$$= \frac{\sum_{i=1}^{M} \mathrm{var}(t_{i,i+1})}{\left(\sum_{i=1}^{M} \langle t_{i,i+1} \rangle\right)^2}, \tag{3.1}$$

where we use the fact that the dwell times are independent random variables, and so their means and variances simply add. Since the $t_{i,i+1}$ are drawn from an exponential distribution with mean $1/\lambda$ and variance $1/\lambda^2$, the CV^2 reduces further as

$$CV^2 = \frac{\sum_{i=1}^{M} \frac{1}{\lambda^2}}{\left(\sum_{i=1}^{M} \frac{1}{\lambda}\right)^2}$$
$$= \frac{\frac{M}{\lambda^2}}{\left(\frac{M}{\lambda}\right)^2}$$
$$= \frac{1}{M}. \tag{3.2}$$

It is trivial to show using simple quadratic minimization that the constant-rate linear chain is optimal over all possible irreversible linear chains since its variance is minimal for a given mean, but the proof that no other branching, loopy, or reversible topologies exist that may have equal or lower variabilities as measured by the CV^2 appears to be less obvious. The main mathematical result of this article is that no other topologies reach a CV^2 of $1/M$. Our proof, detailed in appendix A, proceeds in two steps. First, we prove that the following bound holds for all N-state Markov chains:

$$CV^2 \geq \frac{1}{M}. \tag{3.3}$$

Second, we show that our proposed constant-rate linear chain is the unique solution that saturates this bound.

Confirming the relevance of this theoretical result to natural systems, the best fit of a detailed kinetic model for rhodopsin inactivation to experimental data has exactly the constant-rate linear chain architecture, although for the total generated signal rather than for the lifetime of the system (i.e., in each phosphorylation state, the rate of subsequent phosphorylation is proportional to the state-specific G protein activation rate, and so the mean fraction of the total signal accumulated in each state is constant) (Gibson, Parkes, & Liebman, 2000; Hamer et al., 2003). We postulate that studies of other biological systems for which temporal or total signal reliabilities

are necessary features will uncover similar constant-rate linear topologies. Although not experimentally validated, previous theoretical work (Miller & Wang, 2006) has shown that a constant-rate linear chain could be implemented by the brain as a potential mechanism for measuring an interval of time. Specifically, if a set of strongly intraconnected populations of bistable integrate-and-fire neurons is weakly interconnected in a series, then the total network works like a stochastic clock (i.e., in the presence of noise). By activating the first population through some external input, each subsequent population is activated in turn after some delay given by the strength of the connectivity between the populations. The time from the activation of the first population until the last is equivalent to the hitting time in a linear Markov chain with each population representing a state. Interestingly, Miller and Wang (2006) use this timing mechanism as a way to explain the well-known adherence to Weber's law seen in the behavioral data for interval timing (Gibbon, 1977; Buhusi & Meck, 2005), while our result indicates that this timing architecture is optimal without reference to the data.[4]

4 Numerical Studies of Energy Constraints

Given the inverse relationship between the CV^2 of the hitting time (or the total generated signal) and the number of states for a system with a linear, unidirectional topology (see equation 3.2), it would seem that such a system may be made arbitrarily reliable by increasing the number of states. Why, then, do physical systems not employ a massively large number of states to essentially eliminate trial-to-trial variability in signal generation? The inactivation of activated rhodopsin, for example, appears to be an eight-state (Doan et al., 2006) or nine-state (Hamer et al., 2003) system. Why did nature not increase this number to hundreds of thousands of states? In the case of rhodopsin, one might speculate that the reduction in variability achieved with only eight or nine states is sufficient to render negligible the contribution that the variability in the number of G proteins generated by rhodopsin adds to the total noise in the visual system (i.e., it is small compared to other noise components such as photon shot noise and intrinsic noise in the retinothalamocortical neural circuitry); more generally, for an arbitrary system, it is reasonable to hypothesize that a huge number of states is infeasible due to the cost incurred in maintaining such a large state-space. We will attempt to understand this cost by defining a measure of "energy" over the topology of the system.

[4] In animal and human behavioral data, the variance of a measured interval of time is proportional to the square of its mean (Weber's law). As discussed in section 2.2, all timing mechanisms that can be modeled as Markov chains will have a constant CV^2 (and will thus exhibit Weber's law), but our proof shows that a constant-rate linear mechanism is optimally reliable.

The optimal solution given in the previous section consists entirely of irreversible transitions. We can analyze the energetics of such a topology by borrowing from Arrhenius kinetic theory and considering transitions between states in the Markov chain to be analogous to individual reactions in a chemical process. An irreversible reaction is associated with an infinite energy drop, and thus our optimal topology is an energetic impossibility. Even if one deviates slightly from the optimal solution and sets the transitions to be nearly, but not perfectly, irreversible, then each step is associated with a large, though finite, energy drop. Thus, the total energy required to reset the system following its progression from the first to the final state would equal the sum of all of the energy drops between each pair of states. In this context, it is apparent why a physical system could not maintain the optimal solution with a large number of states N since each additional state would add to the total energy drop across the length of the chain. At some point, the cost of an additional state would outweigh the benefit in terms of reduced variability, and thus the final topology would have a number of states that balances the counteracting goals of variability reduction and conservation of energy resources.

Specifically, in Arrhenius theory, energy differences are proportional to the negative logarithms of the reaction rates (i.e., $\Delta E \propto -\ln \lambda$). In sections 4.2 and 4.3, we define two different energy functions, both consistent with this proportionality concept, but apply it differently and have different interpretations. We then numerically optimize the transition rates of an N-state Markov chain to minimize the CV^2 of the hitting time while holding the total energy E_{tot} constant. This process is repeated for many values of E_{tot} to understand the role that the energy constraints defined by the two different energy functions play in determining the minimally variable solution. As expected and shown in the results here, the CV^2 of the optimal solution increases with decreasing E_{tot}.

4.1 Numerical Methods. Constrained optimization was performed using the optimization toolbox in Matlab. Rather than minimize the CV^2 of the hitting time directly, the variance was minimized while the mean was constrained to be 1, thus making the variance equal to the CV^2. Expressions for the mean and the variance of the hitting time for arbitrary transition rate matrices are given using the known formula for the moments of the hitting time distribution (Norris, 2004; see appendix B for a derivation). In order to implicitly enforce the constraint that the rates must be positive, the rates λ_{ij} were reparameterized in terms of θ_{ij}, where $\theta_{ij} \equiv -\ln \lambda_{ij}$. The variance was then minimized over the new parameters rather than the rates themselves. The gradients of these functions with respect to $\boldsymbol{\theta}$ were also used to speed the convergence of the optimization routine. The gradients of the mean, variance, and energy functions are given in appendix C.

For each value of E_{tot}, parameter optimization was repeated with multiple initial conditions to both discard locally optimal solutions and avoid

numerically unstable parameter regimes. For the second energy function (see section 4.3), local optima were encountered, while none were observed in the parameter space of the first (see section 4.2).

4.2 Energy Cost Function I: Constrain Irreversibility of Transitions. Our first approach at developing a reasonable energy cost function is predicated on the idea that if the values of the reciprocal rates between a single pair of states (e.g., λ_{ij} and λ_{ji} for states i and j) are unequal, then this asymmetry should be penalized, but that the penalty should not depend on the absolute values of the rates themselves. Thus, if two states have equal rates between them (including zero rates), no penalty is incurred, but if the rates differ significantly, then large penalties are applied. In other words, perfectly reversible transitions are not penalized, while perfectly irreversible transitions are infinitely costly. From an energy standpoint, different rates between a pair of states can be thought of as resulting from a quantity analogous to the Gibbs free energy difference between the states. In chemical reactions, reactants and products have intrinsic energy values defined by their specific chemical makeups. The difference between the product and the reactant energies is the Gibbs free energy drop of a reaction. If this value is negative, then the forward reaction rate exceeds the backward rate, and vice versa if the value is positive. By analogy then, we can consider each state in a Markov chain to be associated with an energy, and thus the relative difference between the transition rates in a reciprocal rate pair is due to the energy drop between their corresponding states.[5] For nonzero energy differences, one of the rates is fast because it is associated with a drop in energy, while the other is slow since energy must be invested to achieve the transition. If the energy difference is zero, then both rates are identical. This idea is schematized in Figure 2a where the energy drop ΔE_{ij} between states i and j results in a faster rate λ_{ji} than λ_{ij}.

Thus, the total energy of the system E_{tot} can then be given as the sum of the energy drops between every pair of states:

$$E_{\text{tot}} \equiv \sum_{i,j} |\Delta E_{ij}|, \tag{4.1}$$

where we exclude pairs that contain state N (i.e., since the outgoing rates for transitions away from state N do not affect the hitting time t_{1N} and thus can always be set to equal the reciprocal incoming rates to state N, making those energy drops zero) and count each rate pair only once (because

[5]Note that an arbitrary Markov chain is not conservative (i.e., the path integral of the energy depends on the path), so, although for a pair of states i and j each state can be thought of as having an associated energy, these associated energies may change when i and j are paired with other states in the chain.

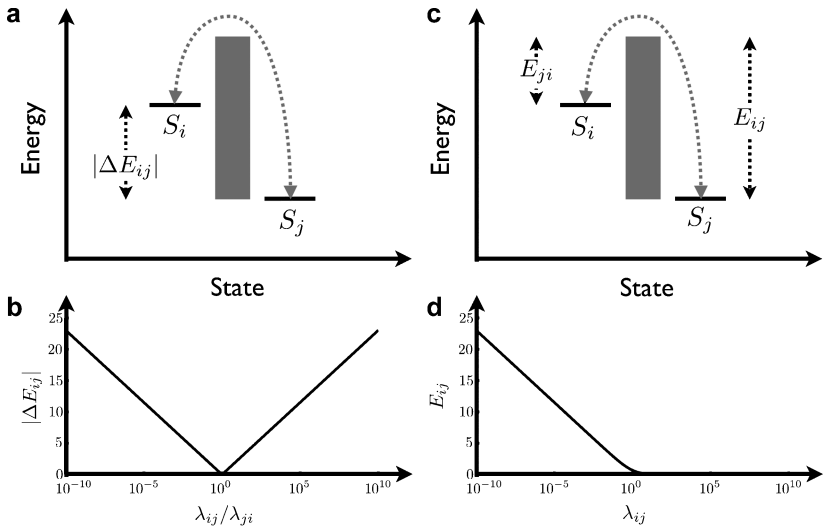

Figure 2: (a) Schematization of the energy associated with the transitions between states i and j for the energy cost function given in equation 4.3. The energies of each state are not equal, and so the transition rates differ (i.e., λ_{ji} from state i to j is faster than λ_{ij} from j to i). For this cost function, the height of the energy barrier in the schematic, which can be thought to represent the absolute values of λ_{ij} and λ_{ji}, does not contribute to E_{tot}, which is affected only by the difference between the energies associated with each state $|\Delta E_{ij}|$. (b) The contribution to the total energy E_{tot} for the pair of transition rates λ_{ij} and λ_{ji} under the first energy function (see equation 4.3). For rates that are nearly identical (i.e., when the ratio $\lambda_{ij}/\lambda_{ji}$ is close to one), $|\Delta E_{ij}|$ is near zero, but it increases logarithmically with the relative difference between the rates. (c) Similar to ***a***, but for the energy cost function given in equation 4.15. In this case, the transition rate λ_{ji} from state i to j is faster, and thus associated with a lower energy barrier, than the rate λ_{ij} from j to i. (d) The contribution to the total energy E_{tot} for the transition rate λ_{ij} under the second energy function (see equation 4.15). For large transition rates, E_{ij} is near zero, but it increases logarithmically for near-zero rates. Note that the abscissas in ***b*** and ***d*** are plotted on a log scale.

$|\Delta E_{ij}| = |\Delta E_{ji}|$). From Arrhenius kinetic theory, the Gibbs free energy difference is proportional to the logarithm of the ratio of the forward and backward reaction rates, and so we use the following definition for the energy drop (plotted in Figure 2b for a single pair of reciprocal rates):

$$\Delta E_{ij} = \ln \frac{\lambda_{ij}}{\lambda_{ji}}. \tag{4.2}$$

Therefore, the complete energy cost function is

$$E_{\text{tot}} = \sum_{i,j} \left| \ln \frac{\lambda_{ij}}{\lambda_{ji}} \right| . \tag{4.3}$$

Note that the individual magnitudes of the rates do not enter into the energy function, only the relative magnitudes between pairs of reciprocal rates.

The results of numerical optimization of the rates λ_{ij} to minimize the CV^2 of the hitting time t_{1N} under the energy function defined in equation 4.3 are given in Figure 3a. At large values of E_{tot}, the optimized solution approaches the asymptotic CV^2 limit of $\frac{1}{M}$ (i.e., the CV^2 of the unconstrained or infinite energy, ideal linear chain; see equation 3.2). As the available energy is decreased, the CV^2 consequently increases until, at $E_{\text{tot}} = 0$, the CV^2 reaches a maximal level of $\frac{1}{\xi(M)}$ (the function $\xi(M)$ will be defined in section 4.2.1).

Upon inspection, for large values of the total energy, the optimized transition rate matrix is seen, as presumed, to be essentially identical to the ideal, infinite energy solution. Specifically, the forward transition rates along the linear chain (i.e., the elements of the lower subdiagonal of the transition rate matrix; see equation 2.3) are all essentially equal to each other, while the remaining rates are all essentially zero. Since the energy function does not penalize symmetric reciprocal rate pairs, the reciprocal rates between nonadjacent states in a linear chain (which are both zero and thus symmetric) would not contribute to the energy. Thus, it would be expected that the optimal solutions found using this energy function would be linear chains, and indeed the minimization procedure does drive rates between nonadjacent states to exactly zero, or, more precisely, the numerical limit of the machine. The only deviations away from the ideal, infinite energy solution occur in the rates along the lower and upper subdiagonals of the transition rate matrix (i.e., the forward and backward rates between adjacent states in the linear chain). As the available energy is decreased, these deviations become more pronounced until the lower and upper subdiagonals become equal to each other at $E_{\text{tot}} = 0$. An analytical treatment of the structure of this zero energy solution is given in section 4.2.1.

An inspection of the transition rate matrix at intermediate values of E_{tot} reveals that as the minimum CV^2 solution deviates between the infinite energy and the zero energy optima, the pairs of forward and backward transition rates between adjacent states become equal, and thus give no contribution to E_{tot}, in sequence, starting from the last pair in the chain ($\lambda_{M-1,M}$ and $\lambda_{M,M-1}$) at some relatively high energy value and ending with the first pair (λ_{12} and λ_{21}) at $E_{\text{tot}} = 0$. This sequential merging of rate pairs, from final pair to first pair, with a decrease in the available energy was a robust result over all network sizes tested. In Figure 3b, for example, the results are shown for the optimization of an eight-state Markov chain. It is clear from the figure that the transition rates deviate smoothly from the

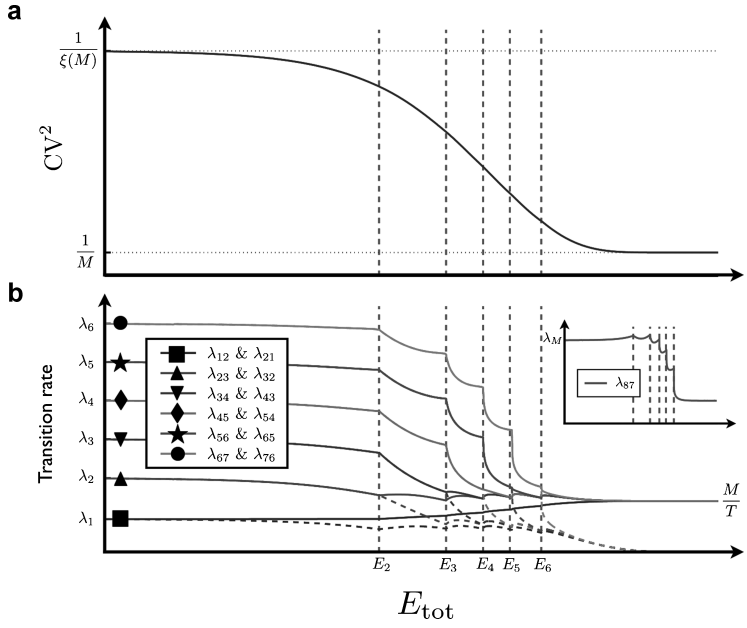

Figure 3: (a) The minimum CV^2 achieved by the numerical optimization procedure as a function of E_{tot} for an eight-state Markov chain using the energy function defined in equation 4.3. At large energy values, the CV^2 approaches the asymptotic infinite energy limit ($\frac{1}{M}$), while at $E_{\mathrm{tot}} = 0$, the CV^2 reaches its maximum value of $\frac{1}{\xi(M)}$ (the function $\xi(M)$ is given by equation 4.7). (b) The transition rate values for the six nonzero pairs of rates between adjacent states along the linear chain (e.g., λ_{12} and λ_{21}, λ_{23} and λ_{32}). At large values of E_{tot}, the forward rates (solid lines) and the backward rates (dashed lines) approach the infinite energy limits of $\frac{M}{T}$ (for $T \equiv \langle t_{1N} \rangle$) and zero, respectively. As the energy is decreased, the rates smoothly deviate from these ideals until, at energy value E_6, the rates λ_{67} and λ_{76} (denoted with the ●) merge and remain merged for all lower energy values. Between E_6 and E_5, the rates again change smoothly until the rates λ_{56} and λ_{65} (★) merge. This pattern repeats itself until ultimately the first rate pair in the chain—λ_{12} and λ_{21} (■)—merges at $E_{\mathrm{tot}} = 0$. The zero energy solutions $\lambda_1, \ldots, \lambda_6$ are given by equation 4.5. Inset: The final, unpaired rate in the chain (λ_{87}) versus E_{tot}. Its zero energy solution λ_M is also given by equation 4.5. As discussed in section 4.2.1, this rate is proportional to M, whereas the zero energy solutions of the paired rates are proportional to i^2, and so λ_M is considerably slower than, for example, λ_{M-1}. Note that the abscissas are plotted on a log scale and that the ordinate in ***b*** is plotted on a square root scale for visual clarity.

infinite energy ideal as E_{tot} is decreased, until the final rate pair (denoted with the ●) merges together at the energy level E_6. At all lower energy values, these two rates remain identical and thus, given the definition of the energy function (see equation 4.3), are noncontributory to E_{tot}. After this first merging, the rates again deviate smoothly with decreasing E_{tot} until the next rate pair (★) merges. This pattern repeats itself until, at $E_{\text{tot}} = 0$, all rate pairs have merged. The value of the unpaired rate at the end of the chain (λ_{87} in this case) as a function of the available energy is shown in the figure inset. At intermediate values of E_{tot}, the as-yet unmerged rate pairs (except for the first rate pair, λ_{12} and λ_{21}) are all identical to each other. That is, all of the forward rates in these unmerged rate pairs are equal, as are all of the backward rates. For example, above E_6 in Figure 3b, the forward rates $\lambda_{32}, \ldots, \lambda_{65}$ are equal, as are the backward rates $\lambda_{23}, \ldots, \lambda_{56}$. In other words, the ▲, ▼, ◆, and ★ traces lie exactly on top of each other. Only the ● traces, corresponding to the rate pair that is actively merging in this energy range, and the ■ traces, corresponding to the first rate pair, deviate from the other forward and backward rates. Between E_5 and E_6, the same unmerged rates continue to be equal except for λ_{56} and λ_{65} (★), which have begun to merge.[6] Essentially this means that the behavior of the system at intermediate values of E_{tot} is insensitive to the current position along the chain anywhere within this set of states with unmerged rate pairs (i.e., the forward and backward rates are the same between all adjacent states in this set).

We can understand why rate pairs should merge by considering the energy function to be analogous to a prior distribution over a set of parameters in a machine-learning-style parameter optimization (e.g., a maximum a posteriori fitting procedure). In this case, the parameters are the logarithms of the ratios of the pairs of rates and the prior distribution is the Laplace, which, in log space, gives the L_1-norm of the parameters (i.e., exactly the definition of the individual terms of E_{tot}; see equation 4.3). As is well known from the machine-learning literature, a Laplace prior or, equivalently, an L_1-norm regularizer, gives rise to a sparse representation where parameters on which the data are least dependent are driven to zero and thus ignored, while those that capture important structural features of the data are spared and remain nonzero (Tibshirani, 1996). In this analogy, E_{tot} is similar to the standard deviation of the prior distribution (or the inverse of the Lagrange multiplier of the regularizer), in that, as it is decreased toward zero, it allows fewer and fewer nonzero log rate ratios to persist. Ultimately, at $E_{\text{tot}} = 0$, the prior distribution overwhelms optimization of the CV^2, and all the pairs of rates are driven to be equal, thus making the

[6] It is not clear why the first rate pair has its own unique behavior. Attempts to analytically solve for the rate values at finite, nonzero energies were unsuccessful, but these numerical results were robust. Similarly, we were unable to determine expressions for the merge-point energies.

log rate ratios zero. This analogy might lead one to consider energy functions that correspond to other prior distributions, but, unlike equation 4.3, functions based on other priors (e.g., a quadratic that would correspond to a gaussian prior) do not result in a clear interpretation of what the energy means, and thus they were not pursued in this work.

One interpretation of the solutions of the optimization procedure at different energy values shown in Figure 3b is as follows. Before a rate pair merges, the corresponding transition can thought of as *directed* with the probability of a forward transition exceeding that of a backward transition. After a merger has taken place, the probabilities of going forward and backward become equal, and we term this behavior *diffusive*. At high values of E_{tot}, the solution is entirely directed, with the system marching from the first state to the final state in sequence. At $E_{\text{tot}} = 0$, the solution is purely diffusive, with the system performing a random walk along the Markov chain. At intermediate energy values, both directed and diffusive regimes coexist. Interestingly, the directed regime always precedes the diffusive regime (i.e., the rate pairs toward the end of the chain merge at higher energy values than those toward the beginning of the chain). Recalling our analogy from the previous paragraph, the first parameters to be driven to zero using a Laplace prior are those that have the least impact in accurately capturing the data. Therefore, in our case, we expect that the first log rate ratios driven to zero are those that have the least impact on minimizing the CV^2 of the hitting time t_{1N}. Thus, our numerical results indicate that at energy levels where a completely directed solution is not possible, it is better, in terms of variability reduction, to first take directed steps and then diffuse rather than diffuse and then take directed steps or mix the two regimes arbitrarily. We present a brief interpretation as to why this structure is favored in section 4.2.2. A schematic of an intermediate energy solution is shown in Figure 4.

4.2.1 Zero Energy or Pure Diffusion Solution. If E_{tot} is zero under the energy function given by equation 4.3, then all pairs of rates λ_{ij} and λ_{ji} are forced to be equal. The rates corresponding to transitions between nonadjacent states in the linear chain (i.e., for $|i - j| \neq 1$) are driven to zero by the optimization of the CV^2, while the adjacent state transition rates remain positive. It is possible to analytically solve for the rates in such a zero energy chain as well as find a semiclosed-form expression for the CV^2 of the hitting time t_{1N} (see appendix D for details).

To simplify notation a bit, since transitions between adjacent states are equal and, between nonadjacent states, zero, we can consider only the rates λ_i for $i \in \{1, \ldots, M\}$ where $\lambda_i \equiv \lambda_{i,i+1} = \lambda_{i+1,i}$. Then the CV^2 can be shown to be

$$\text{CV}^2 = \frac{\mathbf{x}^T \mathbf{Z} \mathbf{x}}{T^2}, \tag{4.4}$$

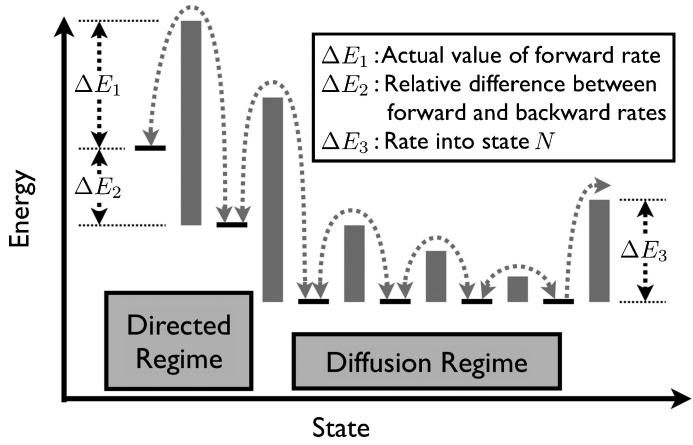

Figure 4: Schematic of a nonzero, finite energy solution for a seven-state Markov chain optimized under the energy function given in equation 4.3. In this case, the first two transitions can be called directed since their forward rates exceed their backward rates. The forward rate λ_{21}, for example, is determined by the height of the energy barrier between states 1 and 2 (i.e., it is proportional to $e^{-\Delta E_1}$. This rate will be a larger value than the backward rate λ_{12} (proportional to $e^{-\Delta E_1 - \Delta E_2}$). On the other hand, the rates between states toward the end of the chain are equal, as represented by states that are at the same energy level. The decreasing energy barriers toward the end of the chain represent the empirical result that the rates increase down the length of the chain (see Figure 3). The larger energy barrier for the final transition to state N represents the result that this rate is much slower than the other rates at the end of the chain. As shown in section 4.2.1 for the $E_{\text{tot}} = 0$ solution, the final rate is a linear function of M, while the other rates grow quadratically (see equation 4.5). Note that the energy level of state N is not represented since there is no reverse transition $N \to M$ to consider.

where we have defined the vector $\mathbf{x}$ as $x_i \equiv \frac{1}{\lambda_i}$, the matrix $\mathbf{Z}$ as $Z_{ij} \equiv \min(i, j)^2$, and, for notational convenience, T as $\langle t_{1N} \rangle$. The λ_i that minimize this CV^2 are

$$\lambda_i = \begin{cases} \frac{\xi(M)}{2T}(4i^2 - 1), & i \neq M \\ \frac{\xi(M)}{T}(2M - 1), & i = M \end{cases}, \tag{4.5}$$

which, substituted back into equation 4.4, give the minimum CV^2 as

$$\mathrm{CV}^2 = \frac{1}{\xi(M)}. \tag{4.6}$$

The function $\xi(M)$ is calculated as

$$\xi(M) = \frac{1}{2}\left(\Psi\left(M + \tfrac{1}{2}\right) + \gamma\right) + \ln 2, \tag{4.7}$$

where $\Psi(x)$ is the digamma function defined as the derivative of the logarithm of the gamma function (i.e., $\Psi(x) \equiv \frac{d}{dx} \ln \Gamma(x)$) and γ is the Euler–Mascheroni constant. Although $\Psi(x)$ has no simple closed-form expression, efficient algorithms exist for determining its values. For $M = 1$, $\xi(1) = 1$, and, as can be shown by asymptotic expansion of $\Psi(x)$, $\xi(M)$ grows logarithmically with M.

Compared to the CV^2 versus number-of-states relationship at infinite energy (see equation 3.2) in the zero energy setting, the CV^2 scales inversely with $\log N$ (see equation 4.6) rather than with N, and thus adding states gives logarithmically less advantage in terms of variability reduction. Furthermore, to achieve even this modest improvement with increasing N, the rates must scale with i^2 (i.e., $\lambda_i \propto 4i^2 - 1$; see equation 4.5), and thus the rates toward the end of the chain need to be $O(N^2 \ln N)$, while those near the start are only $O(\ln N)$. To summarize, then, the zero energy setting has two disadvantages over the infinite energy case. First, for the optimal solution, the CV^2 is inversely proportional to the logarithm of N rather than to N itself, and second, even to achieve this modest variability reduction, a dynamic range of transition rates proportional to N^2 must be maintained.

4.2.2 The Diffusive Regime Follows the Directed Regime. We can understand the numerical result that, at intermediate energy values, the diffusive regime always follows the directed regime by careful consideration of the structure of this solution. First, let us assume that for some value of E_{tot}, the directed regime consists of M_i directed transitions and that the remainder of the system consists of a purely diffusive tail with M_r transitions (where $N = M_i + M_r + 1$). Recalling that transitions to state N are always unpaired, then there are actually $M_i + 1$ directed transitions for this intermediate energy solution: M_i in the directed regime and one at the end of the diffusive tail. However, the energy resources of the system are being devoted solely to maintain the M_i transitions composing the directed regime, since the energy function (see equation 4.3) does not penalize perfectly reversible transitions or transitions leading to state N, such as the one at the end of the diffusive tail.

Now consider if the diffusive regime preceded the directed regime. Then, although there would still be $M_i + 1$ directed transitions (one at the end of the diffusive regime leading into the directed regime and M_i in the directed regime), the energy resources would be apportioned in a new manner. The final transition of the directed regime, since it leads to state N, would not incur any penalty, while the final transition of the diffusive regime would incur a penalty since it now leads to the first state of the

directed regime rather than to state N. In other words, the final transition of the diffusive regime is penalized, as are the first $M_i - 1$ transitions of the directed regime. It is now possible to understand why our numerical optimizations always yield solutions with directed-first, diffusive-second architectures. If the transition rate at the end of the diffusive regime λ_{M_r} (to use the notation introduced in section 4.2.1) is greater than the transition rate at the end of the directed regime λ, then more energy would be required for the diffusive-first architecture, which would penalize λ_{M_r}, than for the directed-first architecture, which does not. Numerically, λ_{M_r} is always seen to be greater than λ, and the following simple analysis also supports this idea.

If we approximate the directed regime as consisting of M_i perfectly irreversible transitions with backward rates of exactly zero, then the directed and diffusive subchains can be considered independently, and thus their variances can be added as

$$\begin{aligned}\mathrm{var}(t_{1N}) &= \mathrm{var}(t_i) + \mathrm{var}(t_r) \\ &= \frac{T_i^2}{M_i} + \frac{T_r^2}{\xi(M_r)},\end{aligned} \tag{4.8}$$

where we have multiplied the expressions for the CV^2 of an ideal linear chain (see equation 3.2) and a zero energy, purely diffusive chain (see equation 4.6) by the squares of the mean processing times for each subchain (T_i and T_r) to get the variances. In order to find the relative rates between the directed and diffusive portions of the chain, we minimize equation 4.8 with respect to the subchain means subject to the constraint that the mean total time is T. This gives

$$T_i = \frac{M_i}{M_i + \xi(M_r)} T \tag{4.9}$$

and

$$T_r = \frac{\xi(M_r)}{M_i + \xi(M_r)} T. \tag{4.10}$$

The forward rate along the directed portion of the chain is thus

$$\begin{aligned}\lambda &= \frac{M_i}{T_i} \\ &= \frac{M_i + \xi(M_r)}{T},\end{aligned} \tag{4.11}$$

and the final rate along the diffusive portion (see equation 4.5) is thus

$$\begin{aligned}\lambda_{M_r} &= \frac{\xi(M_r)}{T_r}(2M_r - 1)\\ &= \frac{M_i + \xi(M_r)}{T}(2M_r - 1)\\ &= \lambda(2M_r - 1).\end{aligned} \tag{4.12}$$

Therefore, for the case of a perfectly irreversible directed regime, the final transition rate of the diffusive regime is always larger than the rate of the directed regime as long as $M_r > 1$. Although this result does not necessarily hold for real intermediate energy solutions (where the directed regime is not perfectly irreversible), this analysis seems to explain the numerical result that the directed-first architecture is optimal.

4.3 Energy Cost Function II: Constrain Incommunicability Between States. Although the results from the previous section are revealing and provide insight into why a physical system might be limited in the number of directed steps it can maintain (as discussed in section 4.4, the diffusive tail found at intermediate values of E_{tot} in the previous section is essentially negligible in terms of variability reduction), it is unclear whether the energy cost function given in equation 4.3 is generally applicable to an arbitrary multistate physical process. Therefore, as a test of the robustness of our results, we defined an additional cost function to determine the behavior of the optimal solution under a different set of constraints. As shown in sections 4.4 and 4.5, the results given by our second cost function, while superficially appearing to be quite different, are in fact analogous to those given in the preceding section.

Our second energy cost function is predicated on the idea that there should be a large penalty for all near-zero rates, or, equivalently, that the maintenance of incommunicability between states should be costly. Although not as neatly tied to a physical energy as the first energy function (which is exactly analogous to the Gibbs free energy; see section 4.2), a small rate of transition between two states can be thought of as resulting from a high "energy" barrier that is preventing the transition from occurring. Inversely, a large rate corresponds to a low energy barrier, and in the limit, one can think of two states with infinite transition rates between them as in fact the same state. This idea is schematized in Figure 2c for the transitions between a pair of states i and j. The energy E_{ji} can be thought of as the energy needed to permit the transition from i to j, and similarly for E_{ij}. Given our intuition regarding the relationship between energies and rates, from the diagram one expects that the rate λ_{ji} is faster than the rate λ_{ij}, since E_{ji} is less than E_{ij}. The total energy in the system E_{tot} can simply be

defined as the sum of energies associated with each transition in the system:

$$E_{\text{tot}} \equiv \sum_{i,j} E_{ij}. \tag{4.13}$$

The energies of the transitions originating in state N are excluded from the preceding sum since their associated transition rates do not affect the hitting time t_{1N} (i.e., transitions away from state N are irrelevant).

To determine a reasonable expression for the individual transition energies, we choose a function such that for near-zero transition rates, $E_{ij} \to \infty$, and, for large transition rates, $E_{ij} \to 0$, which corresponds to our intuition from the previous paragraph. The following definition for the transition energy, plotted in Figure 2d, meets these two conditions:

$$E_{ij} \equiv -\ln \lambda_{ij} + \ln(\lambda_{ij} + 1). \tag{4.14}$$

Therefore, the sceond energy cost function is

$$E_{\text{tot}} = \sum_{i,j} -\ln \lambda_{ij} + \ln(\lambda_{ij} + 1). \tag{4.15}$$

Our results are insensitive to the exact definition of the function as long as the asymptotic behaviors at transition rates of zero and infinity are retained.

The results of numerical optimization of the rates λ_{ij} to minimize the CV^2 for a five-state Markov chain are given in Figure 5a. For large values of E_{tot}, the optimal solution is represented by the ■ trace. This solution asymptotes to $\frac{1}{4}$, which is the theoretical minimum for $N = 5$ (see equation 3.2). Thus, the optimized transition rate matrix looks essentially identical to the ideal, infinite energy solution:

$$\mathbf{A} = \begin{pmatrix} -\frac{4}{T} & 0 & 0 & 0 & 0 \\ \frac{4}{T} & -\frac{4}{T} & 0 & 0 & 0 \\ 0 & \frac{4}{T} & -\frac{4}{T} & 0 & 0 \\ 0 & 0 & \frac{4}{T} & -\frac{4}{T} & 0 \\ 0 & 0 & 0 & \frac{4}{T} & 0 \end{pmatrix}, \tag{4.16}$$

where $T \equiv \langle t_{1N} \rangle$. Since E_{tot} is finite, transition rates of exactly zero are not possible, but for large enough values of E_{tot}, the rates given as zero in equation 4.16 are in fact optimized to near-zero values. Note that this is a different behavior from that seen in the previous section, where reciprocal rates between nonadjacent states in the linear chain were optimized to exactly zero (or, at least, the machine limit) and only the forward and backward rates along the linear chain were affected by the amount of available energy. In this case, all of the rates in the matrix are affected by E_{tot},

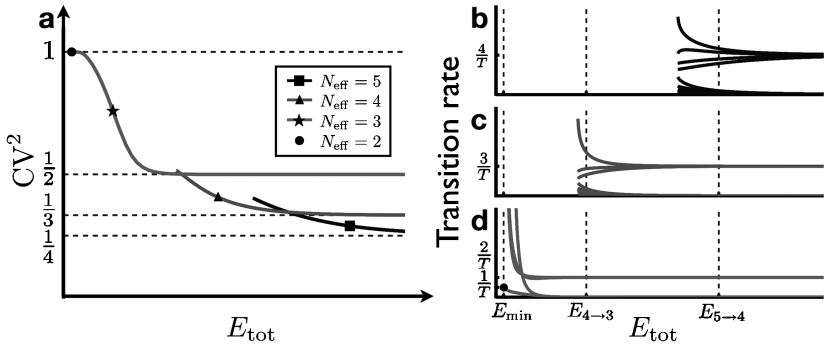

Figure 5: (a) The minimum achievable CV^2 resulting from numerical optimization of the rates of a five-state Markov chain as a function of E_{tot} (given by equation 4.15). The trace marked with the ■ corresponds to a solution close to the five-state linear chain given by equation 4.16, which is the theoretical optimum. As E_{tot} decreases, this solution deviates from the optimal linear chain, and the CV^2 increases from the theoretical limit ($\frac{1}{4}$) until, at the intersection of the ■ and ▲ traces, the solution corresponding to a linear chain with four effective states (two of the five available states have merged; see equation 4.17) becomes optimal. This four-state chain also deviates from its theoretical minimum with decreasing E_{tot} until the linear chain with three effective states (see equation 4.18), shown with the ★, becomes optimal. The minimum energy limit corresponds to a chain with two effective states (see equation 4.19), and this solution is represented with the ●. See the text for a fuller interpretation of these results. (b–d) The optimal transition rates as they vary with E_{tot} for Markov chains with five (***b***), four (***c***), and three (***d***) states. At large energy values, the rates along the lower subdiagonal of the transition rate matrix (i.e., the rates that compose the linear chain) are equal to $\frac{M}{T}$, while all other rates are essentially zero (thus, the upper and lower sets of curves in ***b–d***). These are the optimal solutions. As E_{tot} decreases, the rates deviate from their ideal values and the CV^2 grows as in ***a***. The dashed vertical lines mark the energy values where the CV^2 is equal for numerically optimized chains of different lengths. At $E_{5\to4}$, for example, the minimum achievable CV^2 is the same for both the five- and four-state Markov chains. This is where the ■ and ▲ traces cross in ***a***. It is clear from these crossing points that the linear structure of the shorter chain is essentially fully intact, while that of the longer chain has started to degrade significantly. In ***d***, the three-state Markov chain is seen to converge to the two-state solution (shown with the ●) at E_{min}. One of the rates becomes $\frac{1}{T}$, while the others diverge to infinities (i.e., two of the three states merge).

and the degree to which the rates given as zero in equation 4.16 deviate from true zero depends on the energy. Thus, while in the previous section, the linear architecture is maintained at all values of E_{tot}, optimization under the second energy function would be expected to corrupt the linear structure, and, indeed, as E_{tot} is decreased, all of the near-zero rates, including those

between nonadjacent states in the linear chain, deviate further from zero. Concomitantly, the minimum CV^2, as shown in Figure 5a, is seen to rise as expected.

The ▲ trace in Figure 5a corresponds to another stable solution of the optimization procedure, which, for large values of E_{tot}, is not globally optimal. Inspection of the solution reveals the following transition rate matrix:

$$\mathbf{A} = \begin{pmatrix} -\frac{3}{T} & 0 & \infty & 0 & 0 \\ \frac{3}{T} & -\frac{3}{T} & \infty & 0 & 0 \\ 0 & \frac{3}{2T} & -\infty^2 & \infty & 0 \\ 0 & \frac{3}{2T} & \infty^2 & -\infty & 0 \\ 0 & 0 & \infty & \frac{3}{T} & 0 \end{pmatrix}, \tag{4.17}$$

where, in the third column, ∞^2 is an infinity of a different order from the other infinities in the column (e.g., 10^{100} versus 10^{50}). This hierarchy of infinities is an artifact of the numerical optimization procedure, but the solution is nonetheless revealing. Essentially, states 3 and 4 are merged into a single state in this solution. Whenever the system is in state 3, it immediately transitions to state 4 because the infinity of the higher order (i.e., ∞^2) dominates. From state 4, the system immediately transitions back to state 3, and thus states 3 and 4 are equivalent. There is a single outflow available from this combined state to state 5 with rate $\frac{3}{T}$. Furthermore, there are two sources of input into states 3 and 4, both from state 2, but since the states are combined, this is the same as a single source with a total rate also of $\frac{3}{T}$. Finally, there is an irreversible transition from state 1 to 2 with rate $\frac{3}{T}$. This, then, is exactly the optimal solution for a four-state Markov chain: for large values of E_{tot}, every forward rate is equal to $\frac{3}{T}$, all other rates are near zero, and the CV^2 asymptotes to the theoretical minimum of $\frac{1}{3}$.

The solution to which the ★ trace corresponds can be interpreted similarly to that of the ▲ trace, except that in this case, states 2, 3, and 4 have all merged, and thus the effective number of states is three, not four. For large E_{tot}, the transition matrix approaches

$$\mathbf{A} = \begin{pmatrix} -\frac{2}{T} & \infty & \infty & 0 & 0 \\ \frac{2}{3T} & -\infty^2 & \infty & \infty & 0 \\ \frac{2}{3T} & \infty & -\infty^2 & \infty & 0 \\ \frac{2}{3T} & \infty^2 & \infty^2 & -\infty & 0 \\ 0 & \infty & \infty & \frac{2}{T} & 0 \end{pmatrix}, \tag{4.18}$$

which is the optimal solution for a three-state Markov chain (i.e., the forward rates are $\frac{2}{T}$, the others rates are zero, and the asymptotic CV^2 is $\frac{1}{2}$).

The ● represents the two-state system where the first four states have all merged:

$$\mathbf{A} = \begin{bmatrix} -\infty^2 & \infty & \infty & \infty & 0 \\ \infty & -\infty^2 & \infty & \infty & 0 \\ \infty & \infty & -\infty^2 & \infty & 0 \\ \infty^2 & \infty^2 & \infty^2 & -\infty & 0 \\ \infty & \infty & \infty & \frac{1}{T} & 0 \end{bmatrix}. \tag{4.19}$$

In this case, the constraints on the desired mean and on E_{tot} cannot both be met for arbitrary values of the two variables. There is only one rate available to the optimization procedure in a two-state system, and thus, for mean T, the transition rate must be $\frac{1}{T}$. Therefore, E_{tot} is not a free variable and is locked to $\ln(T+1)$ by equation 4.15. This is another point of difference from the results in the preceding section where the constraint on the mean could still be satisfied when the energy was zero (i.e., when all reciprocal pairs of rates of were equal).

Analysis of the behavior of the solutions with greater than two states as the total energy is decreased is revealing. In all cases, as expected, the minimum values of the CV^2 deviate from the infinite energy asymptotes, but, more interestingly, the curves cross. At the point where the ■ and ▲ traces cross in Figure 5a, for example, the four-state system becomes the globally optimal solution despite the fact that its theoretical minimum at infinite energies is higher than that of the five-state system (i.e., $\frac{1}{3} > \frac{1}{4}$). This can be understood by considering how the available energy that constitutes a given value of E_{tot} is divided up among the rates of the system. The largest penalties are being paid for the near-zero rates, and thus most of the available energy is apportioned to maintain them. As E_{tot} is decreased, maintaining the near-zero rates becomes impossible, and so the network topology begins to deviate significantly from the infinite energy optimum with the CV^2 growing accordingly. This deviation occurs at higher values of E_{tot} for a five-state system than for a four-state system because there are more near-zero rates to maintain for a larger value of N.

Thus, we can understand the trade-off imposed on the system by the energy function given in equation 4.15. The inability to maintain a long, irreversible linear chain at decreasing energy values drives the system to discard states and focus on maintaining a linear chain of a shorter length rather than a branching or loopy chain with more states. Figures 5b to 5d show the degree to which the transition rates deviate from their optimal values for Markov chains of five, four, and three states. The energy thresholds below which a four-state chain outperforms a five-state chain and a three-state chain outperforms a four-state chain are indicated in the figures. It is clear that at these crossing points, the linear structure of the shorter

chain is essentially totally intact, while that of the longer chain has been significantly degraded.

4.4 Comparison of Energy Functions I and II at Finite Nonminimal Energies. The results of the optimizations under the two energy functions in the preceding sections are illuminating. From the theoretical development of the optimal linear Markov chain topology (see section 3), we saw that the CV^2 of the hitting time was equal to $\frac{1}{M}$ (see equation 2.9), which suggests that a physical system can arbitrarily improve its temporal reliability by increasing the number of states. If, however, as in the second energy function (see equation 4.15), a cost is incurred by a system for maintaining zero transition rates (which, functionally, results in incommunicability between states), then, given a finite amount of available energy, we see from section 4.3 that there is some maximum number of states $N_{\max}$ achievable by the system regardless of the total allowable size of the state space N. The CV^2 is thus at best equal to $\frac{1}{M_{\max}}$ where $M_{\max} \equiv N_{\max} - 1$ (i.e., assuming that the linear chain architecture with $N_{\max}$ states is essentially fully intact; see Figure 5).

Alternatively, as in the first energy function (see equation 4.3), by employing a cost incurred for the inclusion of asymmetries between reciprocal pairs of transition rates in the system topology (i.e., irreversible transitions), then, as shown in section 4.2, only a subset of the total number of transitions can be close to irreversible, while the rest must be fully reversible with equal forward and backward transition rates (see Figure 3). Although in this case, a larger N will always result in a lower CV^2, a simple analysis reveals that an effective maximum number of states N_{eff} can be defined that is much less than N itself. If, as in the analysis in section 4.2.2, one assumes that the first M_i transitions form a perfect, irreversible linear chain and that the remainder of the system consists of M_r fully reversible transitions (where $N = M_i + M_r + 1$), then, by combining equations 4.8, 4.9, and 4.10, the CV^2 is given as

$$CV^2 = \frac{1}{M_i + \xi(M_r)}. \tag{4.20}$$

By comparing equation 4.20 with the CV^2 equation for the ideal chain (see equation 3.2), we can equate the denominators and thus define an effective number of states as

$$N_{\text{eff}} \equiv M_i + \xi(M_r) + 1. \tag{4.21}$$

Since $\xi(M)$ grows logarithmically, $N_{\text{eff}} \approx M_i$ unless the magnitude of N is on the order of e^{M_i} or greater. Furthermore, since the available energy dictates what fraction of the N-state chain can be irreversible and thus the

value of M_i, then, in the absence of a massive state space, the energy is the primary determining factor in setting the temporal variability, while the value of N itself is secondary.

From this, it appears that the maximally reliable solutions at finite nonminimal energies under either energy constraint are in fact quite similar. If irreversibility is penalized, then, as long as N is limited enough such that $\xi(M_r) \ll M_i$, the available energy sets the number of states to N_{eff} ($\approx M_i$). If, rather, incommunicability is penalized, then, regardless of how large N is permitted to be, the available energy mandates that the number of states be limited to $N_{\max}$. Furthermore, in both cases, the solutions are essentially irreversible linear chains. The only difference between the two solutions—the diffusive tail at the end of the chain optimized under the first energy function—has minimal impact on the behavior of the system.[7]

Figure 6a shows the relationship between the total allowable number of states N and the minimum achievable CV^2 under the two energy cost functions where the available energies have been tuned such that $M_{\max}$ and M_i are equal, finite, and nonzero. As is clear from Figure 6, although the variability does continue to decrease as N is increased past M_i for the solutions determined under the first energy function (▲), the difference compared to the variability resulting from the second energy function (★) is minimal. The values of the CV^2 as functions of N are shown for two different settings of $M_{\max}$ and M_i, and although the domain of N stretches over several orders of magnitude in the figure, the primary determinants of the CV^2 are the values of $M_{\max}$ and M_i, not N, for both settings.

4.5 Comparison of Energy Functions I and II at Minimal Energies. Although optimization at finite nonminimal energy values under the two cost functions results in similar solutions, at minimal energies, the solutions seem quite different. Recall from section 4.2.1 that at $E_{\text{tot}} = 0$ (the minimal energy value under the first energy function), the CV^2 of the minimally variable solution is equal to $\frac{1}{\xi(M)}$ and thus decreases toward zero with increasing N. Under the second energy function, however, the CV^2 is always equal to 1 for all N at the minimal energy value (recall from section 4.3 that with mean hitting time T, the minimal energy value is $\ln(T+1)$ at which point all of the states have merged leaving $N_{\max}$ equal to 2). These different behaviors as functions of N are shown in Figure 6b as the ▲ and ★, traces respectively. Although $\frac{1}{\xi(M)}$ approaches zero much more slowly than the CV^2 of the infinite energy solution ($\frac{1}{M}$), it is still significant compared to the CV^2 of the minimal energy solution under the second cost function (i.e., 1). However, as discussed in section 4.2.1, to achieve a CV^2 of $\frac{1}{\xi(M)}$, the

[7]Note that many more states may be in the diffusive tail than in the irreversible linear chain portion of the solution, but as long as $\xi(M_r) \ll M_i$, these states fail to remarkably change the reliability of the system.

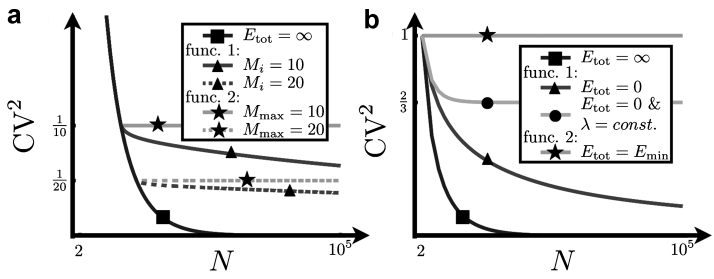

Figure 6: (a) The decrease in the CV^2 as a function of the total allowable size of the state space N for maximally reliable solutions determined under the first (▲) and second (★) energy functions where the energies have been tuned such that $M_i = M_{\max} = 10$ (solid lines) and $M_i = M_{\max} = 20$ (dashed lines). Over a large range of N, the solutions determined under the first energy function are seen to deviate little from those determined under the second despite their long, diffusive tails. The CV^2 in the infinite energy case ($\frac{1}{M}$) is shown as a reference (■). (b) The CV^2 as a function of N for the minimal energy solutions resulting from the first energy function ($\frac{1}{\xi(M)}$; ▲) and the second energy function (1; ★). Unlike in ***a*** for nonminimal energies, these solutions differ quite significantly with N. However, if the range of transition rates is restricted, then the CV^2 of the solution determined under the first energy function does not decrease to zero with increasing N but rather reaches a constant as in the ● trace for a maximally restricted range where all the transition rates are equal (then $CV^2 = \frac{2}{3}$; see the text for details). The infinite energy solution is again shown for comparison. Note that the abscissas are plotted on a log scale.

transition rates near the end of the linear chain must be on the order of N^2 times larger than the values of the rates near the beginning of the chain.

Maintaining such a large dynamic range of rates may be infeasible in the context of a specific system, and so it is reasonable to consider what the advantage is in terms of variability reduction of having such a large range of rates versus having a single nonzero rate (i.e., a constant rate λ for all reciprocal pairs of rates between adjacent states in the linear chain). By substituting a constant rate into equation 4.4 and simplifying, the following can be shown:

$$CV^2 = \frac{2}{3}\left(1 + \frac{1}{N^2 - N}\right). \tag{4.22}$$

This rapidly gives a CV^2 of $\frac{2}{3}$ with increasing N (the ● trace in Figure 6b), and thus it is clear that only with an unrestricted range of rates can the variability be driven arbitrarily close to zero by adding states. If an unrestricted range is not feasible, then even at minimal energy values, the solutions given by the two energy cost functions are not qualitatively different. That is, both

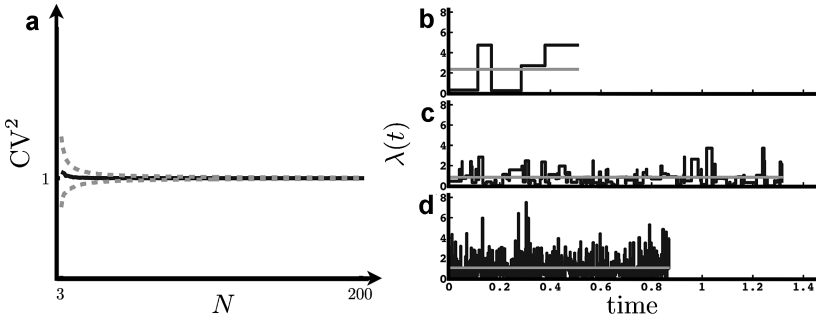

Figure 7: (a) The mean and the $\pm 1\sigma$ deviations of the CV^2 as a function of N, determined empirically from 2000 random transition rate matrices at each value of N, with rates drawn as i.i.d. samples from an exponential distribution. For large N, the distribution of the CV^2 is a delta function at 1. This indicates that random N-state chains are performing identically to two-state chains. (b–d) The instantaneous (in black) and mean (in gray) transition rates to state N as the system transitions between the first $N-1$ states of random (***b***) 10, (***c***) 100, and (***d***) 1000-state chains with transition rates drawn i.i.d. from an exponential distribution with mean 1. The correlation time of the instantaneous transition rate scales as $1/N$, and so, for large N, the mean rate, which is also the mean of the distribution from which the transition rates are drawn, dominates.

result in constant values of the CV^2 that are independent of N (compare the ★ and ● traces in Figure 6b).

4.6 Reliability of Random Transition Rate Matrices. In all cases, under either energy function at any amount of available energy from the minimal possible value to infinity, the goal of the system is to reduce the temporal variability within the given energy constraints, and, as has been shown throughout this article, this is achieved by choosing the maximally reliable network structure among the set of structures that meet the constraints. Thus, it is reasonable to consider the value of choosing an explicit structure rather than an arbitrary random connectivity between a set of states. In Figure 7a, we show the distribution of the CV^2 as a function of N, calculated empirically from 2000 random transition matrices at each value of N, with transition rates λ_{ij} drawn as independent and identically distributed (i.i.d) samples from an exponential distribution. As N increases, the distribution of the CV^2 quickly converges to a delta function centered at one. This is the CV^2 of a minimally reliable two-state system. Numerical studies using other random rate distributions with support on the positive real line (e.g., the uniform, gamma, log-normal) produced the same result.

While initially surprising, the convergence observed in Figure 7a can be easily understood as a consequence of the averaging phenomenon

illustrated in Figures 7b to 7d. These figures show $\lambda(t)$, the instantaneous transition rate to state N, for sample evolutions of random matrices with 10, 100, and 1000 states. If the state of the system at time t is given by $q(t)$, then $\lambda(t)$ equals $\lambda_{Nq(t)}$, the rate of transition from state $q(t)$ to state N. As is clear from the figures, the correlation time of $\lambda(t)$ goes to zero with increasing N (it can be shown to scale as $1/N$), and so a law of large numbers averaging argument can be applied to replace $\lambda(t)$ with its mean (i.e., $\bar{\lambda}$, the mean of the distribution from which the transition rates are drawn). In particular, the time-rescaling theorem (Brown, Barbieri, Ventura, Kass, & Frank, 2002) establishes that the random variable u, defined as

$$u = \int_0^{t_{1N}} \lambda(t) dt, \tag{4.23}$$

is drawn from an exponential distribution with mean one. By the averaging argument, u reduces as follows:

$$\lim_{N\to\infty} u = \bar{\lambda} t_{1N}. \tag{4.24}$$

Finally, since u is distributed exponentially with mean one, then t_{1N} is distributed exponentially with mean $1/\bar{\lambda}$, and thus must have a CV^2 of 1 (confirming the numerical results).

These results make clear the advantage of specific network structure over arbitrary connectivity. A CV^2 of 1 is the same as the reliability of a two-state, one-step process. That is, a random network structure, regardless of the size of N, is minimally reliable.

5 Summary

Many physical systems require reliability in signal generation or temporal processing. We have shown that for systems that may be modeled reasonably well as Markov chains, an irreversible linear chain architecture with the same transition rate between all pairs of adjacent states (see Figure 1b) is uniquely optimal over the entire set of possible network structures in terms of minimizing the variability of the hitting time t_{1N} (equivalently, the architecture that optimally minimizes the variability of the total generated signal F_{1N} is a linear chain with transition rates between pairs of adjacent states that are proportional to the state-specific signal accumulation rates). This result suggests that a physical system could become perfectly reliable by increasing the length of the chain, and so we have attempted to understand why perfect reliability is not observed in natural systems by employing energy cost functions that, depending on the amount of available energy, reduce the possible set of network structures by some degree. Although the two functions are quite different, the optimal network structures resulting

from maximizing the system reliability under the constraints of either function are in fact quite similar. In short, they are irreversible linear chains with a fixed maximum length.

We would predict that natural systems for which temporal or total signal reliabilities are necessary features would be composed of linear chains of finite length, with the length determined by the specific constraints encountered by the system. This prediction has applications across many disciplines of biology. For example, it suggests both that the sequence of openings and closings in the assemblage of ion channels responsible for active membranes processes (i.e., action potentials) and the progression of a dynamical neural network through a set of intermediate attractor states during the cognitive task of estimating an interval of time, should be irreversible linear processes. Our analysis is also useful in the event that some system for which signal reliability is important is found to have a branching or loopy structure. By setting the linear structure as the theoretical limit, deviations from this limit may offer insight into what other counteracting goals physical systems are attempting to meet.

Appendix A: Proof of the Optimality of the Linear, Constant-Rate Architecture

The primary theoretical result of this article is that a linear Markov chain with the same transition rate between all pairs of adjacent states is optimally reliable in terms of having the lowest CV^2 of the hitting time from state 1 to state N of any N-state Markov chain (see Figure 1b). To establish this result, we prove the following two theorems.

Theorem 1 (general bound). *The following inequality holds for all Markov chains of size N and all pairs of states i and j:*

$$CV_{ij}^2 \geq \frac{1}{N-1}, \tag{A.1}$$

where the CV_{ij}^2 is the squared coefficient of variation of t_{ij}, the hitting time from state i to j.

Theorem 2 (existence and uniqueness). *The equality $CV_{ij}^2 = \frac{1}{N-1}$ holds if and only if states i and j are the first and last states of an irreversible, N-state linear chain with the same forward transition rate between all pairs of adjacent states and with state j as a collecting state.*

We employ an inductive argument to prove these theorems. It is trivial to establish the base case of $N = 2$. Since the random variables t_{12} and t_{21} are both exponentially distributed (i.e., with means $1/\lambda_{21}$ and $1/\lambda_{12}$,

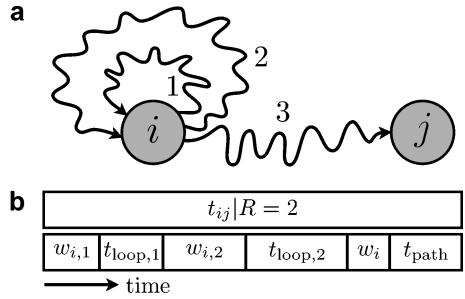

Figure 8: (a) A sample path through an N-state Markov chain conditioned on the assumption that the system loops back to return to the start state i twice ($R = 2$). By conditioning the hitting time t_{ij} on such a path, proof by induction is possible since the time required for the final transit to state j refers, by definition, to a network of size $N - 1$ excluding state i. The wavy lines indicate unspecified paths requiring unspecified numbers of transitions. (b) A schematic of how the hitting time t_{ij} conditioned on two loops ($R = 2$) is decomposed into a set of conditionally independent random variables according to equations A.2 and A.4. The upper box represents the conditional hitting time $t_{ij}|R$, while the smaller boxes represent the proportion of the total time due to, in sequential order from left to right: $w_{i,1}$, the dwell time in state i prior to loop 1; $t_{\text{loop},1}$, the subsequent time required to loop back to i; $w_{i,2}$, the dwell time in i prior to loop 2; $t_{\text{loop},2}$, the subsequent time required to loop back to i; w_i, the dwell time in i prior to the final transit to j; and t_{path}, the time required for the final transit to j. Note that the blocks representing the loop times and the final transit time correspond sequentially to the wavy lines labeled 1, 2, and 3 in ***a***.

respectively), and since the CV^2 for exponential distributions is known to be unity, theorem 1 holds. Furthermore, both t_{12} and t_{21} satisfy the conditions for theorem 2 (i.e., they are hitting times between the first and last states of linear chains with the same transition rates between all pairs of adjacent states), and both saturate the bound. As they are the only hitting times in a two-state network, then theorem 2 also holds for $N = 2$. This establishes a base case and allows us to employ an inductive argument to prove the general result (i.e., by assuming that theorems 1 and 2 hold for networks of size $N - 1$ and proving that they hold for networks of size N).

The logic of the proof is illustrated in Figure 8. We break up the hitting time t_{ij} into a sum of simpler, independent random variables whose means and variances can be easily determined and to which some variance inequalities and the induction principle can be applied. Specifically, t_{ij} can be decomposed into the following sum:

$$t_{ij} = t_{i+l} + t_{\text{path}}, \tag{A.2}$$

where t_{i+l} is the total time the system spends in the start state i and during any loops back to state i, while t_{path} is the time required for the transit along the path through the network to state j after leaving state i for the final time. The important part of this decomposition is that t_{path} is a random variable over a reduced network of size $N-1$ (excluding state i), which will allow us to apply the inductive principle. Since t_{i+l} and t_{path} are independent variables due to the Markov property, their means and variances simply add, and so we can write the following expression for the CV_{ij}^2 of the hitting time t_{ij}:

$$\begin{aligned}\text{CV}_{ij}^2 &\equiv \frac{\text{var}(t_{ij})}{\langle t_{ij}\rangle^2} \\ &= \frac{\text{var}(t_{i+l}) + \text{var}(t_{\text{path}})}{\left(\langle t_{i+l}\rangle + \langle t_{\text{path}}\rangle\right)^2}.\end{aligned} \tag{A.3}$$

To establish theorem 1, this quantity must not be less than $\frac{1}{N-1}$ for any topology, and to establish theorem 2, it must equal $\frac{1}{N-1}$ only for a hitting time t_{ij} where i is the first state and j the final state of a constant-rate, irreversible linear chain of length N. To analyze equation A.3 and thus establish these theorems, we need expressions for the means and variances of the total pre–final transit time t_{i+l} and of the final transit time t_{path}.

A.1 Mean and Variance of the Pre–Final Transit Time t_{i+l}. The statistics of t_{i+l} can be determined by first considering the conditional case where the number of return loops back to state i prior to hitting state j is assumed to be R. Then t_{i+l} (the sum of the total dwell time in start state i plus the total loop time) conditioned on R can be further decomposed as follows:

$$t_{i+l}|R = \left(\sum_{r=1}^{R} w_{i,r} + t_{\text{loop},r}\right) + w_i, \tag{A.4}$$

where $w_{i,r}$ is the dwell time in state i at the beginning of the rth loop, $t_{\text{loop},r}$ is the time required to return to state i for the rth loop, and w_i is the dwell time in state i prior to the final transit to state j.[8] The total hitting time t_{ij} conditioned on R loops is given as the sum of the right-hand side of equation A.4 and t_{path} (see Figure 8 for a schematic when $R = 2$).

The conditional pre–final transit time $t_{i+l}|R$ is simple to analyze since, due to the Markov principle, the random variables on the right-hand side

[8] Note that hitting time variables (e.g., t_{ij}) refer to specific start and end states (i and j, in this case), while t_{loop} and t_{path} refer to specific end states (i and j, respectively), but not specific start states.

of equation A.4 are all conditionally independent given R. Thus, we can calculate the conditional mean and variance as

$$\begin{aligned}\langle t_{i+l}\rangle_{p(t_{i+l}|R)} &= \left(\sum_{r=1}^{R}\langle w_{i,r}\rangle + \langle t_{\mathrm{loop},r}\rangle\right) + \langle w_i\rangle \\ &= (R+1)\langle w_i\rangle + R\langle t_{\mathrm{loop}}\rangle \end{aligned} \tag{A.5}$$

and

$$\begin{aligned}\mathrm{var}(t_{i+l})_{p(t_{i+l}|R)} &= (R+1)\,\mathrm{var}(w_i) + R\,\mathrm{var}\big(t_{\mathrm{loop}}\big) \\ &= (R+1)\langle w_i\rangle^2 + R\,\mathrm{var}\big(t_{\mathrm{loop}}\big), \end{aligned} \tag{A.6}$$

where we have used the notation that $\langle f(x)\rangle_{p(x)}$ and $\mathrm{var}(f(x))_{p(x)}$ are defined, respectively, as the mean and variance of $f(x)$ over the distribution $p(x)$. In equations A.5 and A.6, we are able to drop the r indices since we assume time homogeneity and thus that (1) the distribution over the dwell time in state i prior to loop r ($w_{i,r}$) is the same for every loop r and the same as the distribution over the dwell time in i prior to the final transit to j (w_i), and that (2) the distribution over the time required to loop back to i for the rth loop ($t_{\mathrm{loop},r}$) has the same distribution for each loop. Furthermore, in equation A.6, since the dwell time w_i is an exponentially distributed random variable and thus has a variance equal to the square of its mean, we have substituted $\mathrm{var}(w_i)$ with $\langle w_i\rangle^2$.

To construct expressions for the marginal mean and variance of the pre–final transit time ($\langle t_{i+l}\rangle_{p(t_{i+l})}$ and $\mathrm{var}(t_{i+l})_{p(t_{i+l})}$) from the conditional mean and variance (see equations A.5 and A.6), the following identities are useful:

$$\langle x\rangle_{p(x)} = \langle\langle x\rangle_{p(x|y)}\rangle_{p(y)} \tag{A.7}$$

and

$$\mathrm{var}(x)_{p(x)} = \mathrm{var}\big(\langle x\rangle_{p(x|y)}\big)_{p(y)} + \langle \mathrm{var}(x)_{p(x|y)}\rangle_{p(y)}. \tag{A.8}$$

Thus, for the marginal mean, we have

$$\begin{aligned}\langle t_{i+l}\rangle_{p(t_{i+l})} &= \langle\langle t_{i+l}\rangle_{p(t_{i+l}|R)}\rangle_{p(R)} \\ &= \langle (R+1)\langle w_i\rangle + R\langle t_{\mathrm{loop}}\rangle\rangle_{p(R)} \\ &= (\langle R\rangle + 1)\langle w_i\rangle + \langle R\rangle\langle t_{\mathrm{loop}}\rangle. \end{aligned} \tag{A.9}$$

Similarly, for the marginal variance, we have

$$\begin{aligned}
\operatorname{var}(t_{i+l})_{p(t_{i+l})} &= \operatorname{var}(\langle t_{i+l}\rangle_{p(t_{i+l}|R)})_{p(R)} + \langle \operatorname{var}(t_{i+l})_{p(t_{i+l}|R)}\rangle_{p(R)} \\
&= \operatorname{var}((R+1)\langle w_i\rangle + R\,\langle t_{\text{loop}}\rangle)_{p(R)} \\
&\quad + \langle (R+1)\langle w_i\rangle^2 + R\operatorname{var}(t_{\text{loop}})\rangle_{p(R)} \\
&= \operatorname{var}(R\,\langle w_i\rangle + R\,\langle t_{\text{loop}}\rangle)_{p(R)} \\
&\quad + (\langle R\rangle + 1)\langle w_i\rangle^2 + \langle R\rangle\operatorname{var}(t_{\text{loop}}) \\
&= \operatorname{var}(R)(\langle w_i\rangle + \langle t_{\text{loop}}\rangle)^2 + (\langle R\rangle + 1)\langle w_i\rangle^2 \\
&\quad + \langle R\rangle\operatorname{var}(t_{\text{loop}}) \\
&= \langle R\rangle(\langle R\rangle + 1)(\langle w_i\rangle + \langle t_{\text{loop}}\rangle)^2 \\
&\quad + (\langle R\rangle + 1)\langle w_i\rangle^2 + \langle R\rangle\operatorname{var}(t_{\text{loop}}),
\end{aligned} \tag{A.10}$$

where we have used the fact that the mean dwell time $\langle w_i\rangle$ and the mean loop time $\langle t_{\text{loop}}\rangle$ are both independent of R, and, in the final step, the fact that the number of loops R is given by a shifted geometric distribution, and thus has a variance equal to $\langle R\rangle(\langle R\rangle + 1)$.

By expanding the first term in equation A.10, and then refactorizing and substituting in the expression for the mean (see equation A.9), we can rewrite the variance of t_{i+l} as

$$\begin{aligned}
\operatorname{var}(t_{i+l}) &= \langle R\rangle(\operatorname{var}(t_{\text{loop}}) + \langle t_{\text{loop}}\rangle^2) + ((\langle R\rangle + 1)\langle w_i\rangle \\
&\quad + \langle R\rangle\langle t_{\text{loop}}\rangle)^2 \\
&= \langle R\rangle(\operatorname{var}(t_{\text{loop}}) + \langle t_{\text{loop}}\rangle^2) + \langle t_{i+l}\rangle^2.
\end{aligned} \tag{A.11}$$

A.2 Variance of the Final Transit Time t_{path} in Terms of Hitting Times. In order to get an expression for the variance of the time for the final transit t_{path} in terms of hitting times over reduced networks of size $N-1$ (so that we can use induction), we apply the identity given in equation A.8 to decompose the variance of t_{path} as

$$\begin{aligned}
\operatorname{var}(t_{\text{path}}) &\equiv \operatorname{var}(t_{\text{path}})_{p(t_{\text{path}})} \\
&= \operatorname{var}\left(\langle t_{\text{path}}\rangle_{p(t_{\text{path}}|k)}\right)_{\hat{p}(k)} + \left\langle \operatorname{var}(t_{\text{path}})_{p(t_{\text{path}}|k)}\right\rangle_{\hat{p}(k)},
\end{aligned} \tag{A.12}$$

where state k is the first state visited by the system after state i at the beginning of the final transit from i to j. The random variable t_{path} was

originally defined as the time required for the final transit to state j, and so, given a specific start state, $t_{\text{path}}|k$ is thus the time required for the path from state k to state j, which is exactly the definition of the hitting time t_{kj}. Substituting this equivalence into equation A.12, we get the following:

$$\begin{aligned}\operatorname{var}(t_{\text{path}}) &= \operatorname{var}(\langle t_{kj}\rangle)_{\hat{p}(k)} + \langle \operatorname{var}(t_{kj})\rangle_{\hat{p}(k)} \\ &= \operatorname{var}(\langle t_{kj}\rangle)_{\hat{p}(k)} + \langle \mathrm{CV}_{kj}^2 \langle t_{kj}\rangle^2\rangle_{\hat{p}(k)},\end{aligned} \tag{A.13}$$

where we have replaced the variance of the hitting time t_{kj} with the product of the squares of the CV and the mean, an equivalent formulation.

A.3 Establishing Theorem 1. Returning to the CV_{ij}^2 of the hitting time t_{ij} (see equation A.3), we can replace $\operatorname{var}(t_{i+l})$ with the second term of equation A.11 and $\operatorname{var}(t_{\text{path}})$ with the second term of equation A.13 (the first terms of equations A.11 and A.13 are nonnegative) to state the following bound:

$$\mathrm{CV}_{ij}^2 \geq \frac{\langle t_{i+l}\rangle^2 + \langle \mathrm{CV}_{kj}^2 \langle t_{kj}\rangle^2\rangle_{\hat{p}(k)}}{\left(\langle t_{i+l}\rangle + \langle t_{\text{path}}\rangle\right)^2}. \tag{A.14}$$

Next, we can employ the inductive step of the proof and assume that theorem 1 is true for the reduced networks represented by t_{kj} (recall that these subnetworks are of size $N-1$ since state i is withheld by definition from t_{path} and thus from t_{kj}). This substitution yields the expression

$$\mathrm{CV}_{ij}^2 \geq \frac{\langle t_{i+l}\rangle^2 + \frac{1}{N-2}\langle \langle t_{kj}\rangle^2\rangle_{\hat{p}(k)}}{\left(\langle t_{i+l}\rangle + \langle t_{\text{path}}\rangle\right)^2}. \tag{A.15}$$

We can also use the fact that the second moment of a random variable is not less than the square of its mean (i.e., $\langle x^2\rangle \geq \langle x\rangle^2$) to perform an additional inequality step:

$$\mathrm{CV}_{ij}^2 \geq \frac{\langle t_{i+l}\rangle^2 + \frac{1}{N-2}\langle \langle t_{kj}\rangle\rangle_{\hat{p}(k)}^2}{\left(\langle t_{i+l}\rangle + \langle t_{\text{path}}\rangle\right)^2}. \tag{A.16}$$

Finally, recalling that the hitting time mean $\langle t_{kj}\rangle$ is equivalent to $\langle t_{\text{path}}\rangle_{p(t_{\text{path}}|k)}$, we can use the identity given in equation A.7 to replace $\langle\langle t_{kj}\rangle\rangle_{\hat{p}(k)}$ and state the following final expression for the CV_{ij}^2:

$$\mathrm{CV}_{ij}^2 \geq \frac{\langle t_{i+l}\rangle^2 + \frac{1}{N-2}\langle t_{\text{path}}\rangle^2}{\left(\langle t_{i+l}\rangle + \langle t_{\text{path}}\rangle\right)^2} \tag{A.17}$$

or

$$\mathrm{CV}_{ij}^2 \geq \frac{L^2 + \frac{1}{N-2}P^2}{(L+P)^2}, \tag{A.18}$$

where, for notational simplicity, we have replaced $\langle t_{i+l} \rangle$ and $\langle t_{\mathrm{path}} \rangle$ with L and P, respectively.

Our goal is to establish that the CV_{ij}^2 is not less than $\frac{1}{N-1}$ for all networks of size N. Since equation A.18 is true for all networks, if the minimum value of the ratio on the right-hand side of the inequality is greater than or equal to $\frac{1}{N-1}$, the theorem is proved. The network topology affects this ratio through the values of L and P, and so we minimize with respect to these variables, ignoring whether the joint minimum of L and P corresponds to a realizable Markov chain (i.e., since the unconstrained minimum cannot be greater than any constrained minimum, if the inequality holds for the unconstrained minimum, it must hold for all network structures):

$$\begin{aligned} \mathrm{CV}_{ij}^2 &\geq \min_{\text{networks}} \mathrm{CV}_{ij}^2 \\ &\geq \min_{L,P} \frac{L^2 + \frac{1}{N-2}P^2}{(L+P)^2}. \end{aligned} \tag{A.19}$$

Note that the ratio in equation A.19 is a Rayleigh quotient as a function of the vector $(L, P)^T$ and thus has a known minimum solution (which we derive here for clarity) (Strang, 2003). Equation A.19 gives rise to a Lagrangian minimization as

$$\mathscr{L}(L, P) = L^2 + \frac{1}{N-2}P^2 - \phi(L+P), \tag{A.20}$$

with Lagrange multiplier ϕ. Differentiating with respect to L and P gives expressions for these variables in terms of ϕ as

$$\begin{aligned} \frac{\partial}{\partial L}\mathscr{L}(L, P) &= 2L - \phi \\ L_{\min} &= \frac{\phi}{2} \end{aligned} \tag{A.21}$$

and

$$\begin{aligned} \frac{\partial}{\partial P}\mathscr{L}(L, P) &= \frac{2P}{N-2} - \phi \\ P_{\min} &= \frac{\phi}{2}(N-2). \end{aligned} \tag{A.22}$$

Substituting these expressions back into equation A.19 establishes the proof of the theorem:

$$\begin{aligned}\mathrm{CV}_{ij}^2 &\geq \frac{\left(\frac{\phi}{2}\right)^2 + \frac{1}{N-2}\left(\frac{\phi}{2}(N-2)\right)^2}{\left(\frac{\phi}{2} + \frac{\phi}{2}(N-2)\right)^2} \\ &= \frac{1 + (N-2)}{(1 + (N-2))^2} \\ &= \frac{1}{N-1}. \end{aligned} \tag{A.23}$$

A.4 Establishing Theorem 2. In order to prove that an irreversible linear chain with the same forward transition rate between all adjacent pairs of states is the unique topology that saturates the bound on the CV_{ij}^2 of the hitting time t_{ij} given by theorem 1, we follow a similar inductive approach as in section A.3. To derive the inequality expression for the CV_{ij}^2 given by equation A.18, three successive inequality steps were employed. For equation A.18 to be an equality—a necessary condition for the bound in theorem 1 to also be an equality—each of those steps must be lossless. If the steps are lossless only for the linear chain architecture, then the theorem is proved.

Consider the second inequality step (the inductive step) in section A.3, which results in equation A.15. Recall that the hitting times t_{kj} represent subnetworks of size $N-1$ starting in some set of states $\mathcal{K}$ where every $k \in \mathcal{K}$ is reachable by a single transition from state i. For equation A.15 to be an equality, the CV_{kj}^2 must be equal to $\frac{1}{N-2}$ for all $k \in \mathcal{K}$. By assuming the inductive hypothesis that, for networks of size $N-1$, constant-rate linear chains are the only topologies that saturate the bound, then, for equation A.15 to be an equality, all the states in set $\mathcal{K}$ must be start states of linear chains of length $N-1$. This is clearly possible only if the set $\mathcal{K}$ consists of a single state k.

This constraint, that there is a single state k reachable by direct transition from state i and that this state is the start state of a constant-rate linear chain of length $N-1$, forces the other two inequality steps in section A.3 (see equations A.14 and A.16) to also be equalities. The mean number of loops $\langle R \rangle$ is zero since no loops are possible (i.e., after transitioning from state i to k, the system follows an irreversible linear path to j, which never returns to i), and so the first term of equation A.11 is zero. Furthermore, the variance of $\langle t_{kj} \rangle$ is zero since there is only one $k \in \mathcal{K}$, and so the first term of equation A.13 is also zero. Thus, the substitutions comprising the first inequality step (see equation A.14) are lossless. Similarly, since there is only one $k \in \mathcal{K}$, the second moment of $\langle t_{kj} \rangle$ equals the square of its mean, which makes the substitution resulting in the final inequality (see equation A.16) also lossless.

Therefore, if and only if the network topology is such that state k is the only state reachable from state i and state k is the start state of a constant-rate linear chain of length $N-1$, then the following holds:

$$\mathrm{CV}_{ij}^2 = \frac{\langle t_{i+l}\rangle^2 + \frac{1}{N-2}\langle t_{\mathrm{path}}\rangle^2}{\left(\langle t_{i+l}\rangle + \langle t_{\mathrm{path}}\rangle\right)^2}. \tag{A.24}$$

We can simplify this expression by noting (1) that $R = 0$ and so $\langle t_{i+l}\rangle = \langle w_i\rangle = 1/\lambda_{ki}$ where λ_{ki} is the transition rate from state i to state k, (2) that there is only one $k \in \mathcal{K}$, and so $\langle t_{\mathrm{path}}\rangle = \langle t_{kj}\rangle$, and (3) that t_{kj} represents a constant-rate linear chain of length $N-1$, and so its mean hitting time will be the number of transitions divided by the constant transition rate (i.e., $\langle t_{kj}\rangle = \frac{N-2}{\lambda}$ for constant rate λ):

$$\begin{aligned}\mathrm{CV}_{ij}^2 &= \frac{\left(\frac{1}{\lambda_{ki}}\right)^2 + \frac{1}{N-2}\left(\frac{N-2}{\lambda}\right)^2}{\left(\frac{1}{\lambda_{ki}} + \frac{N-2}{\lambda}\right)^2} \\ &= \frac{\lambda^2 + (N-2)\lambda_{ki}^2}{\left(\lambda + (N-2)\lambda_{ki}\right)^2}.\end{aligned} \tag{A.25}$$

As in section A.3, to determine the relative values of λ_{ki} and λ that minimize the CV_{ij}^2, we can define the following Lagrangian:

$$\mathscr{L}(\lambda, \lambda_{ki}) = \lambda^2 + (N-2)\lambda_{ki}^2 - \phi\left(\lambda + (N-2)\lambda_{ki}\right). \tag{A.26}$$

Differentiating by each variable and substituting out the Lagrange multiplier ϕ establishes the theorem:

$$\begin{aligned}\frac{\partial}{\partial\lambda}\mathscr{L}(\lambda, \lambda_{ki}) &= 2\lambda - \phi \\ \phi &= 2\lambda,\end{aligned} \tag{A.27}$$

$$\begin{aligned}\frac{\partial}{\partial\lambda_{ki}}\mathscr{L}(\lambda, \lambda_{ki}) &= 2(N-2)\lambda_{ki} - \phi(N-2) \\ \lambda_{ki} &= \frac{\phi}{2} \\ \lambda_{ki} &= \lambda.\end{aligned} \tag{A.28}$$

All transition rates are equal, and so the uniqueness proof is complete. An N-state Markov chain saturates the bound given in theorem 1 if and only if it is an irreversible linear chain with the same forward transition rate between all pairs of adjacent states. Furthermore, the bound is saturated only for the hitting time from the first to the last state in the chain (see Figure 1b).

Appendix B: The Moments of t_{ij}

For clarity, we give a derivation of the explicit formula for the nth moment of the hitting time t_{ij} from state i to j for the Markov chain given by the transition rate matrix $\mathbf{A}_j$. The subscript j in $\mathbf{A}_j$ is used to denote the fact that the jth column of the matrix is a vector of all zeros (i.e., j is a collecting state). For the purposes of this derivation, we assume that the underlying transition rate matrix $\mathbf{A}$, without the connections away from j removed, represents a Markov chain for which all states are reachable from all other states in a finite amount of time. In other words, $\mathbf{A}$ is assumed to be ergodic (although the resulting formulas still hold if this assumption is relaxed). Substituting t for t_{ij} to simplify notation and using the expression for the probability distribution of t_{ij} given in equation 2.6, we have

$$\begin{aligned}\langle t^n \rangle &= \int_0^\infty t^n p(t) dt \\ &= \int_0^\infty t^n \mathbf{e}_j^T \mathbf{A}_j e^{\mathbf{A}_j t} \mathbf{e}_i dt \\ &= \mathbf{e}_j^T \int_0^\infty t^n e^{\mathbf{A}_j t} dt \, \mathbf{A}_j \mathbf{e}_i, \end{aligned} \tag{B.1}$$

where we have used the fact that a matrix commutes with the exponentiation of itself.

In order to evaluate this integral, it is convenient to construct an identity matrix defined in terms of $\mathbf{A}_j$ and a pseudoinverse of $\mathbf{A}_j$, $\mathbf{P_A}$. If the eigenvalue decomposition of $\mathbf{A}_j$ is $\mathbf{RDL}$ (with $\mathbf{L} = \mathbf{R}^{-1}$), then $\mathbf{P_A} \equiv \mathbf{RP_DL}$ where $\mathbf{P_D}$ is a diagonal matrix composed of the inverse eigenvalues of $\mathbf{A}_j$ except for the jth entry which is left at zero (the jth eigenvalue of $\mathbf{A}_j$ is zero). In matrix notation, $\mathbf{P_D}$ is given as

$$\mathbf{P_D} \equiv \left(\mathbf{D} + \mathbf{e}_j \mathbf{e}_j^T\right)^{-1} - \mathbf{e}_j \mathbf{e}_j^T, \tag{B.2}$$

which gives $\mathbf{P_A}$ as

$$\begin{aligned}\mathbf{P_A} &\equiv \mathbf{RP_DL} \\ &= \mathbf{R}[\left(\mathbf{D} + \mathbf{e}_j \mathbf{e}_j^T\right)^{-1} - \mathbf{e}_j \mathbf{e}_j^T]\mathbf{L} \\ &= \left[\mathbf{R}\left(\mathbf{D} + \mathbf{e}_j \mathbf{e}_j^T\right)\mathbf{L}\right]^{-1} - \mathbf{Re}_j \mathbf{e}_j^T \mathbf{L} \\ &= \left(\mathbf{A}_j + \mathbf{e}_j \mathbf{1}^T\right)^{-1} - \mathbf{e}_j \mathbf{1}^T, \end{aligned} \tag{B.3}$$

where, in the final step, we have used the fact that the jth column of $\mathbf{R}$ (the jth right eigenvector of $\mathbf{A}_j$) is $\mathbf{e}_j$ (since the jth column of $\mathbf{A}_j$ is $\mathbf{0}$) and the fact that the jth row of $\mathbf{L}$ (the jth left eigenvector) is $\mathbf{1}^T \equiv [1, \ldots, 1]$ (since the columns of $\mathbf{A}_j$ all sum to 0). Thus, $\mathbf{R}\mathbf{e}_j = \mathbf{e}_j$ and $\mathbf{e}_j^T \mathbf{L} = \mathbf{1}^T$.[9]

To construct an appropriate identity matrix, we calculate the product of $\mathbf{A}_j$ and its pseudoinverse as

$$\begin{aligned}\mathbf{A}_j \mathbf{P}_\mathbf{A} &= \mathbf{RDL} \cdot \mathbf{RP_D L} \\ &= \mathbf{R}\left(\mathbf{DP_D}\right)\mathbf{L} \\ &= \mathbf{R}\left(\mathbf{I} - \mathbf{e}_j \mathbf{e}_j^T\right)\mathbf{L} \\ &= \mathbf{I} - \mathbf{e}_j \mathbf{1}^T \end{aligned} \tag{B.4}$$

where we have used the fact that $\mathbf{DP_D}$ is an identity matrix except for a zero in the jth diagonal entry (due to the noninverted zero eigenvalue). Furthermore, it is trivial to show that $\mathbf{A}_j^n \mathbf{P}_\mathbf{A}^n = \mathbf{A}_j \mathbf{P}_\mathbf{A}$ for any positive integer n (since $\mathbf{A}_j \mathbf{e}_j = \mathbf{0}$), and so we have derived the following expression for the identity matrix:

$$\mathbf{I} = \mathbf{A}_j^n \mathbf{P}_\mathbf{A}^n + \mathbf{e}_j \mathbf{1}^T. \tag{B.5}$$

Finally, this allows us to restate the transition rate matrix as

$$\begin{aligned}\mathbf{A}_j &= \mathbf{A}_j \cdot \mathbf{I} \\ &= \mathbf{A}_j \left(\mathbf{A}_j^n \mathbf{P}_\mathbf{A}^n + \mathbf{e}_j \mathbf{1}^T\right) \\ &= \mathbf{A}_j^{n+1} \mathbf{P}_\mathbf{A}^n, \end{aligned} \tag{B.6}$$

where again we have used the fact that $\mathbf{e}_j$ is the eigenvector of $\mathbf{A}_j$ associated with the zero eigenvalue.

Substituting equation B.6 and the eigenvalue decomposition of $\mathbf{A}_j$ into equation B.1 gives

$$\begin{aligned}\langle t^n \rangle &= \mathbf{e}_j^T \int_0^\infty t^n e^{\mathbf{A}_j t} dt \, \mathbf{A}_j^{n+1} \mathbf{P}_\mathbf{A}^n \mathbf{e}_i \\ &= \mathbf{e}_j^T \int_0^\infty t^n e^{\mathbf{RDL}t} dt \, \left(\mathbf{RDL}\right)^{n+1} \mathbf{P}_\mathbf{A}^n \mathbf{e}_i \end{aligned}$$

[9] Note that $\mathbf{P}_\mathbf{A}$ defined in this manner does not meet all of the conditions of the unique Moore-Penrose pseudoinverse (Penrose & Todd, 1955). Though the equalities $\mathbf{A}_j \mathbf{P}_\mathbf{A} \mathbf{A}_j = \mathbf{A}_j$ and $\mathbf{P}_\mathbf{A} \mathbf{A}_j \mathbf{P}_\mathbf{A} = \mathbf{P}_\mathbf{A}$ hold (as long as $\mathbf{A}_j$ is an appropriately structured transition rate matrix with j as the unique collecting state), the products $\mathbf{P}_\mathbf{A} \mathbf{A}_j$ and $\mathbf{A}_j \mathbf{P}_\mathbf{A}$ are not symmetric matrices (as they are for the Moore-Penrose pseudoinverse).

$$= \mathbf{e}_j^T \int_0^\infty t^n \mathbf{R} e^{\mathbf{D}t} \mathbf{L} dt \, \mathbf{R} \mathbf{D}^{n+1} \mathbf{L} \mathbf{P}_{\mathbf{A}}^n \mathbf{e}_i$$

$$= \mathbf{e}_j^T \mathbf{R} \int_0^\infty t^n e^{\mathbf{D}t} \mathbf{D}^{n+1} dt \, \mathbf{L} \mathbf{P}_{\mathbf{A}}^n \mathbf{e}_i. \tag{B.7}$$

The off-diagonal elements of the integral portion of equation B.7 are zero, as is the jth diagonal element (i.e., the zero eigenvalue of $\mathbf{A}_j$ associated with eigenvector $\mathbf{e}_j$). The kth diagonal element of the integral for $k \neq j$ is given by

$$\left[\int_0^\infty t^n e^{\mathbf{D}t} \mathbf{D}^{n+1} dt \right]_k = \eta_k^{n+1} \int_0^\infty t^n e^{\eta_k t} dt, \tag{B.8}$$

where η_k is the kth eigenvalue. These integrals are analytically tractable:

$$\begin{aligned} \left[\int_0^\infty t^n e^{\mathbf{D}t} \mathbf{D}^{n+1} dt \right]_k &= \eta_k^{n+1} \int_0^\infty \frac{d^n}{d\eta_k^n} e^{\eta_k t} dt \\ &= \eta_k^{n+1} \frac{d^n}{d\eta_k^n} \int_0^\infty e^{\eta_k t} dt \\ &= \eta_k^{n+1} \frac{d^n}{d\eta_k^n} \left(-\frac{1}{\eta_k} \right) \\ &= \eta_k^{n+1} (-1)^{n+1} \frac{n!}{\eta_k^{n+1}} \\ &= (-1)^{n+1} n! \end{aligned} \tag{B.9}$$

where we have used the fact that all of the eigenvalues of $\mathbf{A}_j$ except the jth are strictly negative, which is a result of the following argument. Since $\mathbf{A}_j$ is a properly structured transition rate matrix for a continuous-time Markov chain, there exists a finite, positive dt such that $\mathbf{I} + \mathbf{A}_j dt$ is a properly structured transition probability matrix for a discrete time Markov chain. We can rewrite this probability matrix as $\mathbf{R}(\mathbf{I} + \mathbf{D}dt)\mathbf{L}$ and use the Perron-Frobenius theorem, which states that the eigenvalues of transition probability matrices (i.e., the entries of $\mathbf{I} + \mathbf{D}dt$) are all less than or equal to one (Poole, 2006). Furthermore, since we assumed that the underlying Markov chain $\mathbf{A}$ is ergodic, the Perron-Frobenius theorem asserts that exactly one of the eigenvalues is equal to one. Thus, it is clear that one of the entries of $\mathbf{D}$ is equal to zero and the rest are negative.

Substituting the result from equation B.9 back into equation B.7, gives the final expression for the moments of the hitting time:

$$\begin{aligned}\langle t^n \rangle &= (-1)^{n+1} n! \mathbf{e}_j^T \mathbf{R} \left(\mathbf{I} - \mathbf{e}_j \mathbf{e}_j^T \right) \mathbf{L} \mathbf{P}_{\mathbf{A}}^n \mathbf{e}_i \\ &= (-1)^{n+1} n! \mathbf{e}_j^T \left(\mathbf{I} - \mathbf{e}_j \mathbf{1}^T \right) \mathbf{P}_{\mathbf{A}}^n \mathbf{e}_i \\ &= (-1)^n n! \left(\mathbf{1} - \mathbf{e}_j \right)^T \mathbf{P}_{\mathbf{A}}^n \mathbf{e}_i . \end{aligned} \tag{B.10}$$

As an alternative to the preceding somewhat cumbersome algebra, it is also possible to use an intuitive argument to find the analytic expression for the first moment (mean) of the hitting time (Norris, 2004). With the expression for the first moment known, the higher-order moments can then be derived using Siegert's recursion (Siegert, 1951; Karlin & Taylor, 1981).

Appendix C: The Gradients of the Mean, Variance, and Energy Cost Functions

From appendix B, the expressions for the mean and variance of the hitting time t_{1N} are given as

$$\langle t_{1N} \rangle = - \left(\mathbf{1} - \mathbf{e}_N \right)^T \mathbf{P}_{\mathbf{A}} \mathbf{e}_1 \tag{C.1}$$

and

$$\mathrm{var}(t_{1N}) = 2 \left(\mathbf{1} - \mathbf{e}_N \right)^T \mathbf{P}_{\mathbf{A}}^2 \mathbf{e}_1 - \langle t_{1N} \rangle^2 . \tag{C.2}$$

The definition of $\mathbf{P}_{\mathbf{A}}$ (see equation B.3) and the expression for the derivative of an inverse matrix ($\partial \mathbf{M}^{-1} = -\mathbf{M}^{-1} \left(\partial \mathbf{M} \right) \mathbf{M}^{-1}$) give the following:

$$\begin{aligned}\partial \mathbf{P}_{\mathbf{A}} &= \partial [\left(\mathbf{A}_N + \mathbf{e}_N \mathbf{1}^T \right)^{-1} - \mathbf{e}_N \mathbf{1}^T] \\ &= - \left(\mathbf{A}_N + \mathbf{e}_N \mathbf{1}^T \right)^{-1} \partial \mathbf{A} \left(\mathbf{A}_N + \mathbf{e}_N \mathbf{1}^T \right)^{-1} \\ &= - [\left(\mathbf{A}_N + \mathbf{e}_N \mathbf{1}^T \right)^{-1} - \mathbf{e}_N \mathbf{1}^T] \partial \mathbf{A} [\left(\mathbf{A}_N + \mathbf{e}_N \mathbf{1}^T \right)^{-1} - \mathbf{e}_N \mathbf{1}^T] \\ &= - \mathbf{P}_{\mathbf{A}} \partial \mathbf{A} \mathbf{P}_{\mathbf{A}}, \end{aligned} \tag{C.3}$$

where we have defined $\partial \mathbf{A}$ as the derivative of $\mathbf{A}_N$ with respect to the variable of interest, and have used the fact that $\mathbf{e}_N$ and $\mathbf{1}^T$ are the right and left eigenvectors of $\mathbf{A}_N$ associated with the zero eigenvalue and thus that both $\left(\partial \mathbf{A} \right) \mathbf{e}_N$ and $\mathbf{1}^T \partial \mathbf{A}$ are zero. Therefore, the gradients of the mean and variance with respect to the optimization parameters θ_{ij} (where $\theta_{ij} \equiv - \ln \lambda_{ij}$ for transition rate λ_{ij}) can be shown to be

$$\frac{\partial}{\partial \theta_{ij}} \langle t_{1N} \rangle = \left(\mathbf{1} - \mathbf{e}_N \right)^T \mathbf{P}_{\mathbf{A}} \partial \mathbf{A}^{ij} \mathbf{P}_{\mathbf{A}} \mathbf{e}_1 , \tag{C.4}$$

and

$$\frac{\partial}{\partial\theta_{ij}}\mathrm{var}(t_{1N}) = 2\,(\mathbf{1}-\mathbf{e}_N)^T \times\mathbf{P}_\mathbf{A}\left\{\left[\mathbf{e}_1\,(\mathbf{1}-\mathbf{e}_N)^T-\mathbf{I}\right]\mathbf{P}_\mathbf{A}\partial\mathbf{A}^{ij}-\partial\mathbf{A}^{ij}\mathbf{P}_\mathbf{A}\right\}\mathbf{P}_\mathbf{A}\mathbf{e}_1, \quad \text{(C.5)}$$

where the element in the kth row and lth column of the differential matrix $\partial\mathbf{A}^{ij}$ is given by

$$[\partial\mathbf{A}^{ij}]_{kl} = \begin{cases} -\lambda_{ij}, & k=i \text{ and } l=j \\ \lambda_{ij}, & k=j \text{ and } l=j \\ 0, & \text{otherwise} \end{cases}. \quad \text{(C.6)}$$

Energy cost function I (see section 4.2), given as

$$E_{\mathrm{tot}} = \sum_{i,j}\left|\ln\frac{\lambda_{ij}}{\lambda_{ji}}\right|, \quad \text{(C.7)}$$

has a gradient of

$$\frac{\partial}{\partial\theta_{ij}}E_{\mathrm{tot}} = \begin{cases} 1, & \lambda_{ij}<\lambda_{ji} \\ -1, & \lambda_{ij}>\lambda_{ji} \\ 0, & \lambda_{ij}=\lambda_{ji} \end{cases}, \quad \text{(C.8)}$$

while energy cost function II (see section 4.3), given as

$$E_{\mathrm{tot}} = \sum_{i,j} -\ln\lambda_{ij}+\ln\left(\lambda_{ij}+1\right), \quad \text{(C.9)}$$

has a gradient of

$$\frac{\partial}{\partial\theta_{ij}}E_{\mathrm{tot}} = \frac{1}{1+\lambda_{ij}}. \quad \text{(C.10)}$$

Appendix D: Derivation of Pure Diffusion Solution

At $E_{\mathrm{tot}}=0$, under the energy function given in equation 4.3, it is possible to analytically solve for the transition rates that minimize the CV^2 of the hitting time. First, note that all pairs of reciprocal rates must be equal (since the energy is zero), and furthermore, that all pairs of rates between nonadjacent states are equal to zero. Thus, to simplify notation, we shall consider only the rates λ_i for $i\in\{1,\ldots,M\}$ where $\lambda_i\equiv\lambda_{i,i+1}=\lambda_{i+1,i}$ and $M\equiv N-1$. This

yields the following transition rate matrix:

$$\mathbf{A}_N \equiv \begin{bmatrix} -\lambda_1 & \lambda_1 & 0 & \cdots & 0 & 0 \\ \lambda_1 & -\lambda_1 - \lambda_2 & \lambda_2 & \cdots & 0 & 0 \\ 0 & \lambda_2 & -\lambda_2 - \lambda_3 & \cdots & 0 & 0 \\ \vdots & \vdots & \vdots & \ddots & \vdots & \vdots \\ 0 & 0 & 0 & \cdots & -\lambda_{M-1} - \lambda_M & 0 \\ 0 & 0 & 0 & \cdots & \lambda_M & 0 \end{bmatrix}. \tag{D.1}$$

From our general definitions of the moments of t_{1N} for abitrary Markov chains (see equation B.10), we have, respectively,

$$\langle t_{1N} \rangle = -(\mathbf{1} - \mathbf{e}_N)^T \mathbf{P}_\mathbf{A} \mathbf{e}_1 \tag{D.2}$$

and

$$\begin{aligned} \mathrm{var}(t_{1N}) &= \langle t_{1N}^2 \rangle - \langle t_{1N} \rangle^2 \\ &= 2(\mathbf{1} - \mathbf{e}_N)^T \mathbf{P}_\mathbf{A}^2 \mathbf{e}_1 - \langle t_{1N} \rangle^2, \end{aligned} \tag{D.3}$$

where $\mathbf{P}_\mathbf{A} \equiv \left(\mathbf{A}_N + \mathbf{e}_N \mathbf{1}^T\right)^{-1} - \mathbf{e}_N \mathbf{1}^T$ (see equation B.3) as before. For the specific tridiagonal matrix $\mathbf{A}_N$ given in equation D.1, $\mathbf{P}_\mathbf{A}$ can be shown to be

$$\mathbf{P}_\mathbf{A} = \begin{bmatrix} -\sum_{i\geq 1} \frac{1}{\lambda_i} & -\sum_{i\geq 2} \frac{1}{\lambda_i} & -\sum_{i\geq 3} \frac{1}{\lambda_i} & \cdots & -\frac{1}{\lambda_M} & 0 \\ -\sum_{i\geq 2} \frac{1}{\lambda_i} & -\sum_{i\geq 2} \frac{1}{\lambda_i} & -\sum_{i\geq 3} \frac{1}{\lambda_i} & \cdots & -\frac{1}{\lambda_M} & 0 \\ -\sum_{i\geq 3} \frac{1}{\lambda_i} & -\sum_{i\geq 3} \frac{1}{\lambda_i} & -\sum_{i\geq 3} \frac{1}{\lambda_i} & \cdots & -\frac{1}{\lambda_M} & 0 \\ \vdots & \vdots & \vdots & \ddots & \vdots & \vdots \\ -\frac{1}{\lambda_M} & -\frac{1}{\lambda_M} & -\frac{1}{\lambda_M} & \cdots & -\frac{1}{\lambda_M} & 0 \\ \sum_{i\geq 1} \frac{i}{\lambda_i} & \sum_{i\geq 2} \frac{i}{\lambda_i} & \sum_{i\geq 3} \frac{i}{\lambda_i} & \cdots & \frac{M}{\lambda_M} & 0 \end{bmatrix}, \tag{D.4}$$

from which, with a bit more manipulation, we can give expressions for the mean and variance as follows:

$$\begin{aligned} \langle t_{1N} \rangle &= \sum_{i=1}^{M} \frac{i}{\lambda_i} \\ &= \mathbf{x}^T \mathbf{z} \end{aligned} \tag{D.5}$$

and

$$\begin{aligned}\mathrm{var}(t_{1N}) &= \sum_{i=1}^{M} \frac{1}{\lambda_i} \sum_{j=1}^{M} \frac{\min(i,\, j)^2}{\lambda_j} \\ &= \mathbf{x}^T \mathbf{Z} \mathbf{x}, \end{aligned} \tag{D.6}$$

where we have defined the vectors $\mathbf{x}$ and $\mathbf{z}$ as $x_i \equiv \frac{1}{\lambda_i}$ and $z_i \equiv i$, respectively, and the matrix $\mathbf{Z}$ as $Z_{ij} \equiv \min(i,\, j)^2$.

Finding $\mathbf{x}$, and thus the rates λ_i, that minimizes the CV^2 of t_{1N} is equivalent to employing Lagrangian optimization to minimize the variance while holding the mean constant at $\langle t_{1N} \rangle$. This gives the following simple linear algebra problem:

$$\mathbf{x}_{\min} = \arg\min_{\mathbf{x}} \left(\mathbf{x}^T \mathbf{Z} \mathbf{x} - \alpha \mathbf{x}^T \mathbf{z} \right), \tag{D.7}$$

where $\mathbf{x}_{\min}$ is guaranteed to be the unique optimum since $\mathbf{Z}$ is positive definite (see section D.1) and the constraint is linear. Thus, the solution can be found by setting the gradient to zero:

$$\begin{aligned} 0 &= \nabla_{\mathbf{x}} \left(\mathbf{x}^T \mathbf{Z} \mathbf{x} - \alpha \mathbf{x}^T \mathbf{z} \right) \Big|_{\mathbf{x}=\mathbf{x}_{\min}} \\ 0 &= \mathbf{Z} \mathbf{x}_{\min} - \alpha \mathbf{z} \\ \mathbf{x}_{\min} &= \alpha \mathbf{Z}^{-1} \mathbf{z}. \end{aligned} \tag{D.8}$$

Note that we did not enforce that the elements of $\mathbf{x}$ (and thus the rates λ_i) be positive under this optimization. However, if the solution $\mathbf{x}_{\min}$ has all positive entries, as will be shown, then this additional constraint can be ignored.

Some algebra reveals that $\mathbf{Z}^{-1}$ is a symmetric tridiagonal matrix with diagonal elements

$$[\mathbf{Z}^{-1}]_{ii} = \begin{cases} \dfrac{4i}{4i^2 - 1}, & i < M \\ \dfrac{1}{2M - 1}, & i = M \end{cases}, \tag{D.9}$$

and subdiagonal elements

$$[\mathbf{Z}^{-1}]_{i,i+1} = [\mathbf{Z}^{-1}]_{i+1,i} = -\frac{1}{2i + 1}, \quad i < M. \tag{D.10}$$

Substituting this inverse into the expression for the minimum above (see equation D.8) yields, for $i < M$,

$$\begin{aligned}
[\mathbf{x}_{\min}]_i &= \alpha[\mathbf{Z}^{-1}\mathbf{z}]_i \\
&= \alpha \begin{pmatrix} -\frac{1}{2i-1} & \frac{4i}{4i^2-1} & -\frac{1}{2i+1} \end{pmatrix} \begin{pmatrix} i-1 \\ i \\ i+1 \end{pmatrix} \\
&= \frac{2\alpha}{4i^2-1}, \qquad \text{(D.11)}
\end{aligned}$$

and, for $i = M$,

$$\begin{aligned}
[\mathbf{x}_{\min}]_M &= \alpha \left[\mathbf{Z}^{-1}\mathbf{z}\right]_M \\
&= \alpha \begin{pmatrix} -\frac{1}{2M-1} & \frac{1}{2M-1} \end{pmatrix} \begin{pmatrix} M-1 \\ M \end{pmatrix} \\
&= \frac{\alpha}{2M-1}. \qquad \text{(D.12)}
\end{aligned}$$

For positive values of α—corresponding to positive values of $\langle t_{1N} \rangle$—all of the elements of $\mathbf{x}_{\min}$ are positive, and thus this solution is reasonable. Therefore, the following rates minimize the processing time variability for a zero-energy, purely diffusive system:

$$\frac{1}{\lambda_i} = \begin{cases} \frac{2\alpha}{4i^2-1}, & i \neq M \\ \frac{\alpha}{2M-1}, & i = M \end{cases}. \qquad \text{(D.13)}$$

To determine α from $\langle t_{1N} \rangle$, we substitute the solution (see equation D.13) into the expression for the mean given by equation D.5:

$$\begin{aligned}
\langle t_{1N} \rangle &= \sum_{i=1}^{M} \frac{i}{\lambda_i} \\
&= \left(\sum_{i=1}^{M-1} \frac{2\alpha i}{4i^2-1} \right) + \frac{\alpha M}{2M-1} + \left(\frac{2\alpha M}{4M^2-1} - \frac{2\alpha M}{4M^2-1} \right) \\
&= \alpha \left[\left(\sum_{i=1}^{M} \frac{2i}{4i^2-1} \right) + \frac{M}{2M+1} \right] \\
&= \alpha \left[\left(\sum_{i=1}^{M} \frac{2i}{4i^2-1} \right) + \left(\sum_{i=1}^{M} \frac{1}{4i^2-1} \right) \right]
\end{aligned}$$

$$
\begin{aligned}
&= \alpha \left(\sum_{i=1}^{M} \frac{2i+1}{4i^2-1} \right) \\
&= \alpha \left(\sum_{i=1}^{M} \frac{1}{2i-1} \right) \\
&= \alpha \, \xi(M),
\end{aligned} \tag{D.14}
$$

where we have defined $\xi(M) \equiv \sum_{i=1}^{M} \frac{1}{2i-1}$ and have taken advantage of the following series identity (which can easily be shown by induction):

$$
\frac{M}{2M+1} = \sum_{i=1}^{M} \frac{1}{4i^2-1}. \tag{D.15}
$$

Our introduced function, $\xi(M)$, can be shown to have the following closed-form solution (Abramowitz & Stegun, 1964):

$$
\xi(M) = \frac{1}{2} \left(\Psi \left(M + \tfrac{1}{2} \right) + \gamma \right) + \ln 2, \tag{D.16}
$$

where $\Psi(x)$ is the digamma function defined as the derivative of the logarithm of the gamma function (i.e., $\Psi(x) \equiv \frac{d}{dx} \ln \Gamma(x)$) and γ is the Euler–Mascheroni constant.

From equation D.14, we see that

$$
\alpha = \frac{\langle t_{1N} \rangle}{\xi(M)}, \tag{D.17}
$$

which can be substituted back into equation D.13 to give the optimal rates in terms of $\langle t_{1N} \rangle$ rather than α:

$$
\frac{1}{\lambda_i} = \begin{cases} \dfrac{2\langle t_{1N} \rangle}{\xi(M)\,(4i^2-1)}, & i \neq M \\ \dfrac{\langle t_{1N} \rangle}{\xi(M)\,(2M-1)}, & i = M \end{cases}. \tag{D.18}
$$

It is now possible to find an expression for the CV^2 in terms of M and $\langle t_{1N} \rangle$. From the derivation of equation D.8, we have

$$
\mathbf{Z}\mathbf{x}_{\min} = \alpha \mathbf{z}, \tag{D.19}
$$

which can be substituted into equation D.6 to get

$$\mathrm{var}(t_{1N}) = \alpha \mathbf{x}_{\min}^T \mathbf{z}. \tag{D.20}$$

Finally, using the expressions for the mean and for α (see equations D.5 and D.17), we obtain the following result:

$$\begin{aligned} \mathrm{CV}^2 &= \frac{\alpha \langle t_{1N} \rangle}{\langle t_{1N} \rangle^2} \\ &= \frac{1}{\xi(M)} \\ &= \frac{1}{\xi(N-1)}, \end{aligned} \tag{D.21}$$

where we revert to a notation using the number of states N.

D.1 The Matrix $\mathbf{Z}_{ij} \equiv \min(i, j)^2$ Is Positive Definite. The $M \times M$ matrix $\mathbf{Z}$, where $\mathbf{Z}_{ij} \equiv \min(i, j)^2$, is positive definite. First, note the following identity:

$$n^2 = \sum_{i=1}^{n} 2i - 1, \tag{D.22}$$

which can be easily proven inductively. Now let us define a set of vectors $\sqrt{\mathbf{2i-1}}$ for $i = 1, \ldots, M$ where vector $\sqrt{\mathbf{2i-1}}$ consists of $i-1$ zeros followed by $M - i + 1$ elements all having the value $\sqrt{\mathbf{2i-1}}$—for example,

$$\mathbf{1} \equiv (1, \ldots, 1)^T, \tag{D.23}$$

$$\sqrt{\mathbf{3}} \equiv (0, \sqrt{3}, \ldots, \sqrt{3})^T, \tag{D.24}$$

and

$$\sqrt{\mathbf{5}} \equiv (0, 0, \sqrt{5}, \ldots, \sqrt{5})^T. \tag{D.25}$$

From the identity given in equation D.22, $\mathbf{Z}$ can be rewritten as the following sum of outer products:

$$\mathbf{Z} = \sum_{i=1}^{M} \sqrt{\mathbf{2i-1}} \sqrt{\mathbf{2i-1}}^T. \tag{D.26}$$

Now consider $\mathbf{x}^T\mathbf{Z}\mathbf{x}$ for arbitrary nonzero $\mathbf{x}$. We have

$$\begin{aligned}\mathbf{x}^{\mathbf{T}}\mathbf{Z}\mathbf{x} &= \mathbf{x}^{\mathbf{T}}\left(\sum_{i=1}^{M}\sqrt{\mathbf{2}\boldsymbol{i}-\mathbf{1}}\sqrt{\mathbf{2}\boldsymbol{i}-\mathbf{1}}^{T}\right)\mathbf{x}\\ &= \sum_{i=1}^{M}\mathbf{x}^{\mathbf{T}}\sqrt{\mathbf{2}\boldsymbol{i}-\mathbf{1}}\sqrt{\mathbf{2}\boldsymbol{i}-\mathbf{1}}^{T}\mathbf{x}\\ &= \sum_{i=1}^{M}\left(\sqrt{\mathbf{2}\boldsymbol{i}-\mathbf{1}}^{T}\mathbf{x}\right)^{2}, \end{aligned} \tag{D.27}$$

which must be nonnegative since it is a sum of squares. Furthermore, the $\sqrt{\mathbf{2}\boldsymbol{i}-\mathbf{1}}$ vectors are linearly independent and, since there are M of them, they form a basis. Since the projection of an arbitrary nonzero vector on at least one basis vector must be nonzero, one of the terms in the sum in equation D.27 must be positive. Thus, we have

$$\mathbf{x}^T\mathbf{Z}\mathbf{x} > 0, \tag{D.28}$$

and so $\mathbf{Z}$ is positive definite.

Acknowledgments

S.E. acknowledges the N.I.H. Medical Scientist Training Program and the Columbia University M.D.-Ph.D. Program for supporting this research. L.P. is supported by an NSF CAREER award, an Alfred P. Sloan Research Fellowship, and a McKnight Scholar award. We thank B. Bialek, S. Ganguli, L. Abbott, T. Toyoizumi, X. Pitkow, and other members of the Center for Theoretical Neuroscience at Columbia University for many helpful discussions.

References

Abramowitz, M., & Stegun, I. (Eds.). (1964). *Handbook of mathematical functions with formulas, graphs, and mathematical tables*. Washington, DC: U.S. Government Printing Office.

Brown, E., Barbieri, R., Ventura, V., Kass, R., & Frank, L. (2002). The time-rescaling theorem and its application to neural spike train data analysis. *Neural Comput., 14*, 325–346.

Buhusi, C., & Meck, W. (2005). Functional and neural mechanisms of interval timing. *Nature Reviews Neuroscience*, *6*, 755–765.

Doan, T., Mendez, A., Detwiler, P., Chen, J., & Rieke, F. (2006). Multiple phosphorylation sites confer reproducibility of the rod's single-photon responses. *Science, 313*, 530–533.

Edmonds, B., Gibb, A., & Colquhoun, D. (1995a). Mechanisms of activation of glutamate receptors and the time course of excitatory synaptic currents. *Annual Review of Physiology, 57*, 495–519.

Edmonds, B., Gibb, A., & Colquhoun, D. (1995b). Mechanisms of activation of muscle nicotinic acetylcholine receptors and the time course of endplate currents. *Annual Review of Physiology, 57*, 469–493.

Gibbon, J. (1977). Scalar expectancy theory and Weber's law in animal timing. *Psychological Review, 84*, 279–325.

Gibson, S., Parkes, J., & Liebman, P. (2000). Phosphorylation modulates the affinity of light-activated rhodopsin for G protein and arrestin. *Biochemistry, 39*, 5738–5749.

Hamer, R., Nicholas, S., Tranchina, D., Liebman, P., & Lamb, T. (2003). Multiple steps of phosphorylation of activated rhodopsin can account for the reproducibility of vertebrate rod single-photon responses. *Journal of General Physiology, 122*(4), 419–444.

Kandel, E., Schwartz, J., & Jessell, T. (Eds.). (2000). *Principles of neural science* (4th ed.). New York: McGraw-Hill.

Karlin, S., & Taylor, H. (1981). *A first course in stochastic processes*. New York: Academic Press.

Locasale, J. W., & Chakraborty, A. K. (2008). Regulation of signal duration and the statistical dynamics of kinase activation by scaffold proteins. *PLoS Comput. Biol., 4*(6), e1000099.

Miller, P., & Wang, X. (2006). Stability of discrete memory states to stochastic fluctuations in neuronal systems. *Chaos, 16*, 026109.

Norris, J. (2004). *Markov chains*. Cambridge: Cambridge University Press.

Olivier, E., Davare, M., Andres, M., & Fadiga, L. (2007). Precision grasping in humans: From motor control to cognition. *Current Opinion in Neurobiology, 17*, 644–648.

Penrose, R., & Todd, J. (1955). A generalized inverse for matrices. *Mathematical Proceedings of the Cambridge Philosophical Society, 51*, 406–413.

Poole, D. (2006). *Linear algebra: A modern introduction* (2nd ed.). Belmont, CA: Thomson Brooks/Cole.

Reppert, S., & Weaver, D. (2002). Coordination of circadian timing in mammals. *Nature, 418*, 935–941.

Rieke, F., & Baylor, D. (1998). Origin of reproducibility in the responses of retinal rods to single photons. *Biophys. J., 75*, 1836–1857.

Siegert, A. (1951). On the first passage time probability problem. *Physical Review, 81*, 617–623.

Strang, G. (2003). *Introduction to linear algebra*. (3rd ed.). Wellesley, MA: Wellesley-Cambridge.

Tibshirani, R. (1996). Regression shrinkage and selection via the LASSO. *Journal of the Royal Statistical Society, Series B, 58*, 267–288.

Received August 18, 2008; accepted November 12, 2008.